A circuit of protein-protein regulatory interactions enables polarity establishment in a bacterium

Wei Zhao[1], Samuel W. Duvall[1], Kimberly A. Kowallis[1], Dylan T. Tomares[1], Haley N. Petitjean[1], W. Seth Childers[1]

[1]Department of Chemistry, University of Pittsburgh, Pittsburgh, PA 15260, USA.

Lead Contact: W. Seth Childers; E-mail: wschild@pitt.edu

Abstract

Asymmetric cell division generates specialized daughter cells that play a variety of roles including tissue morphogenesis in eukaryotes and pathogenesis in bacteria. In the gram-negative bacterium *Caulobacter crescentus*, asymmetric localization of two biochemically distinct signaling hubs at opposite cell poles provides the foundation for asymmetric cell division. Through a set of genetic, synthetic biology and biochemical approaches we have characterized the regulatory interactions between three scaffolding proteins. These studies have revealed that the scaffold protein PodJ functions as a central mediator for organizing the new cell signaling hub, including promoting bipolarization of the central developmental scaffold protein PopZ. In addition, we identified that the old pole scaffold SpmX serves as a negative regulator of PodJ subcellular accumulation. These two scaffold-scaffold regulatory interactions serve as the core of an integrated cell polarization circuit that is layered on top of the cell-cycle circuitry to coordinate cell differentiation and asymmetric cell division.

Keywords: *Caulobacter crescentus*; asymmetric cell division; cell polarity; scaffold proteins; PodJ; PopZ; cell-cycle regulation; PleC; SpmX

Introduction

The earliest stage of an asymmetric cell division is the unequal inheritance of cell fate determinants. While models of eukaryotic cell polarity have been developed (Chau et al., 2012) it remains unclear what mechanisms are employed by bacteria to achieve polarity (McAdams and Shapiro, 2009). The degree of asymmetry of cell division in the bacterial kingdom has only been sparsely examined, however broad implications in pathogenesis (Van der Henst et al., 2013) and persister cell development (Aakre and Laub, 2012) have been reported.

Caulobacter crescentus is a well-established bacterial model organism for examining how bacterial cells divide asymmetrically (Shapiro et al., 1971). The cell division results in two morphologically and functionally distinct cells (Figure 1A): a motile swarmer cell that is incapable of chromosome replication and a sessile stalked cell that initiates replication once per cell-cycle (Bergé and Viollier, 2018; Curtis and Brun, 2010; Lasker et al., 2016). These two cell-types utilize bimodal survival strategies, including distinct responses to heavy metal stress (Lawaree et al., 2016) and differences in buoyancy (Ardissone et al., 2014). The swarmer cell can differentiate into stalked cell by shedding the flagellum and initiating stalk biogenesis and chromosome replication (Figure 1A). Genetic studies have revealed that *C. crescentus* bacteria do not use the primary cell polarity regulators that drive eukaryotic stem cell division, but use a set of self-assembled scaffolding proteins to achieve these goals (Bergé and Viollier, 2018; Lasker et al., 2016; Tsokos and Laub, 2012).

Much of the developmental differences between the *C. crescentus* swarmer and stalked cell-types is coordinated by the CtrA signaling pathway which regulates more than 90 genes associated with flagella and stalk biogenesis, chromosome replication and cell wall growth (Laub et al., 2002). Asymmetric activation of the CtrA signaling pathway arises due to the asymmetric

47 localization of two compositionally and functionally distinct signaling complexes (Lasker et al.,
48 2016; Matroule et al., 2004). In pre-divisional cells the new cell pole signaling hub is composed
49 of three scaffolding proteins (TipN (Huitema et al., 2006; Lam et al., 2006), PodJ (Hinz et al.,
50 2003; Viollier et al., 2002) and PopZ (Bowman et al., 2008; Ebersbach et al., 2008)) and eight
51 key signaling proteins (PleC, CpaE, DivL, DivK, PleD, PopA, MopJ and CckA) that function
52 together to activate the CtrA pathway via phosphorylation (Lasker et al., 2016). The old cell pole
53 is composed of two scaffolds (SpmX (Radhakrishnan et al., 2008) and PopZ) and three signaling
54 proteins (DivJ, DivK and PleD) that work as a concerted system to deactivate CtrA through both
55 dephosphorylation and proteolysis (Lasker et al., 2016). The positioning of these complexes
56 prior to division ensures that the daughter cells differentially regulate CtrA and develop as
57 unique cell-types (Figure 1A). Moreover, as newborn swarmer cells differentiate into stalked
58 cells, their inherited PodJ-rich signaling hub undergoes compositional remodeling to become a
59 SpmX-rich signaling hub (Figure 1A). Central questions remain regarding how *C. crescentus*
60 cells establish, maintain and remodel cell polarity to coordinate asymmetric cell division with the
61 cell-cycle.

62 The PopZ scaffolding protein plays a central role in organizing the two organelle-like
63 signaling complexes, as it binds directly to seven client proteins (Holmes et al., 2016). However,
64 PopZ is a common scaffold shared by both the new and old cell pole signaling hubs. This raises
65 the question of how PopZ prevents mixing of signaling hubs when it switches from a monopolar
66 to a bipolar localization pattern as cell develop from a swarmer cell into a pre-divisional cell
67 (Figure 1A). Studies have shown that timing of new cell pole accumulation of PopZ is correlated
68 with the initiation of replication (Laloux and Jacobs-Wagner, 2013; Mera et al., 2014). Studies
69 have indicated that the coordination of cell cycle and cell polarity could be mediated by proteins

whose transcription is activated by DnaA and repressed by CtrA (Figure 1B) (Crymes et al., 1999). Two proteins contribute to PopZ bipolarization, ZitP (Berge et al., 2016) and TipN (Laloux and Jacobs-Wagner, 2013), however each of these studies suggest that redundant factors promote PopZ's new cell pole binding. One potential candidate protein is the new cell pole signaling scaffold PodJ, whose transcription upregulated at the same time as the initiation of replication (Figure 1B) (Crymes et al., 1999) and is proteolyzed prior to the swarmer-to-stalk transition (Chen et al., 2006; Curtis et al., 2012). Meanwhile, PodJ is required for establishment of cell polarity and asymmetric cell division (Hinz et al., 2003). PodJ directly or indirectly recruits the PleC kinase (Curtis et al., 2012; Hinz et al., 2003; Viollier et al., 2002), the pilus assembly protein CpaE (Viollier et al., 2002), and the ClpXP protease adaptor protein PopA (Duerig et al., 2009; Ozaki et al., 2014) to the new cell pole.

The PodJ scaffold domain architecture includes a N-terminal cytosolic domain composed of a coiled-coil rich region (Lawler et al., 2006) that is adjacent to an intrinsically disordered region (Figure 2A). The disordered region is comprised of two compositionally distinct sections. Residues 471-588 are rich in proline, serine and glutamic acid residues with a net charge of -18. While residues 589-642 are rich in serine, glycine and lysine residues with a net charge of +10. The C-terminal end passes through the membrane into the periplasm and contains a tetrapeptide co-repeat domain and a peptidoglycan binding domain (Lawler et al., 2006). The periplasmic domains coordinate pili biogenesis at the new cell pole and have been shown to be dispensable for PodJ localization at the cell pole (Lawler et al., 2006). PodJ's cytoplasmic domains have been implicated directly or indirectly with the recruitment of signaling proteins that activate the CtrA pathway (PleC (Curtis et al., 2012; Lawler et al., 2006; Viollier et al., 2002), DivL (Curtis et al., 2012)), initiate pili biogenesis (CpaE (Curtis et al., 2012; Viollier et al., 2002)) and localize the

93 holdfast complex (HfaB (Hardy et al., 2010)). Previous domain analysis has implicated a portion
94 of the intrinsically disordered domain and the periplasmic domain in new cell pole targeting of
95 PodJ (Lawler et al., 2006). However it remains unclear if this cell pole recruitment is dependent
96 upon other polarity proteins (e.g. TipN or PopZ), and more broadly how the PodJ contributes to
97 polarity establishment. Here we apply a combination of heterologous reconstitution experiments,
98 genetics, quantitative cell biology and biochemical assays to map the regulatory interactions
99 between three central scaffolding proteins (PopZ, PodJ and SpmX) that can account for exquisite
100 cell polarity observed in asymmetrically dividing *C. crescentus* cells.
101
102 **Results**
103 ***PodJ expression level is critical for the maintenance of cell polarity***
104 Spatiotemporal PodJ protein abundance is highly regulated at the levels of transcription (Crymes
105 et al., 1999) and proteolysis (Chen et al., 2006; Chen et al., 2005; Curtis et al., 2012) (Figure
106 1B). Expression of sfGFP-PodJ at a 0.03% xylose induction level in a Δ*podJ* strain resulted in
107 PodJ accumulation at the new cell pole (Figure 1C and 1D). During the swarmer-to-stalked cell
108 transition, the PodJ focus at the old cell pole diminished, while a new PodJ focus accumulated at
109 the new cell pole (Figure 1C, Figure S1A, Movie S1). This localization pattern is consistent with
110 previous immunofluorescence microscopy observations (Hinz et al., 2003; Viollier et al., 2002).
111 In contrast, overexpression of PodJ resulted in cell filamentation and several small ectopic cell
112 poles that were observed in 53% of cells (Figure 1E), each containing a PodJ focus (Figure 1E).
113 These data indicate that strict regulation of PodJ protein expression levels in *C. crescentus* is
114 critical for maintenance of cell polarity and rod morphology.
115 ***PodJ monopolar subcellular accumulation is dependent upon the old cell pole complex***

Live cell imaging of sfGFP-PodJ in Δ*popZ*, Δ*spmX*, Δ*tipN* or Δ*pleC* strains showed that PodJ accumulated at the cell poles in each of these deletion strain (Figure 2B). Therefore, PodJ accumulation as a focus was independent of other known scaffold proteins. However, we did observe that PodJ subcellular position was dependent upon PopZ or SpmX, as the percentage of cells containing monopolar PodJ significantly reduced from 82% in wild-type cell to 35% for Δ*popZ*, and 9% for Δ*spmX* (Figure 2B). Because deletion of *spmX* results in long-chain cell phenotype in *C. crescentus* (Radhakrishnan et al., 2008), the accumulated PodJ foci also occupied each constriction sites. Collectively, these results suggest that PodJ accumulation as a focus is independent of other known scaffold proteins. However, the subcellular positioning of PodJ is dependent directly or indirectly upon the scaffolding proteins PopZ and SpmX.

PodJ accumulates at the cell poles in E. coli independent of specific C. crescentus proteins

To further test if PodJ subcellular accumulation was independent of other *C. crescentus* specific factors, we heterologously expressed PodJ in *Escherichia coli* BL21 cells. Notably, the γ-proteobacterium *E. coli* is highly divergent from the α-proteobacterium *C. crescentus* and does not contain any clear homologs of the *C. crescentus* scaffolding proteins or new cell pole signaling proteins. YFP-PodJ accumulated at both cell poles in *E. coli* (Figure 2C), suggesting that PodJ cell pole accumulation was independent of known *C. crescentus* polarity proteins. Co-expression of YFP-PodJ together with inclusion body marker IbpA-mCherry (Lindner et al., 2008) demonstrated that PodJ did not co-localize with inclusion bodies in *E. coli* (Figure S3B). Moreover, YFP-PodJ localized as a bipolar pattern in about 80% of *E. coli* cells (Figure 2C), which differs from its monopolar localization pattern in *C. crescentus*. These results suggest that possible negative or positive regulators may promote the monopolar accumulation of PodJ in *C. crescentus*.

To identify a minimal cell pole accumulating domain, we screened a set of 21 PodJ domain deletion variants for their capabilities to maintain cell pole accumulation (Figure 2D, Figure S2). Amongst this set, the construct representing the PerP-cleaved form of PodJ that lacks the periplasmic domains, PodJΔperi, accumulated at the cell poles similar to the wild-type PodJ in *E. coli* (Figure 2D), consistent with earlier studies (Lawler et al., 2006). Deletion of the intrinsically disordered PSE-rich region or CC4-6 does not affect PodJ subcellular accumulation (Figure S3). In contrast, the PodJ localization pattern gradually changed from bipolar to diffuse when we truncated the coiled-coil (CC) domains 1 to 3 (Figure 2D), indicating that residues 1-249 were critical for cell pole accumulation of PodJ.

PodJ self-assembled into a high order oligomer in vitro

Since PodJ accumulated at the cell poles independent of other known scaffolding proteins *in vivo*, we hypothesized that PodJ is a self-assembled protein. We therefore purified the cytoplasmic portion of PodJ, PodJ(1-635), and analyzed the protein through native gel analysis (Figure 2F). The result showed PodJ oligomerization into an array of large oligomeric complexes ranging in size from 720-1048 kDa. Further analytical size exclusion chromatography of PodJ(1-635) indicated PodJ oligomers ranging in size from: 71 kDa (monomer), 194 kDa (dimer), and > 650 kDa (> 8-mer) (Figure 2G). These results indicate that PodJ is a self-assembled scaffolding proteins, and that subcellular localization may be dependent upon coiled-coil multivalent interactions.

PodJ is the central organizer of new cell pole assembly

Previous studies have suggested that PodJ could serve as a scaffolding protein as PleC (Viollier et al., 2002), CpaE (Ozaki et al., 2014; Viollier et al., 2002), and PopA (Ozaki et al., 2014)) all require PodJ for subcellular accumulation. However, it remains elusive if these dependencies are

due to a direct or indirect recruitment by PodJ. To address these questions, we screened 17 cell-cycle regulatory proteins (Figure S2A) for their capacity to co-localize with PodJ upon heterologous co-expression in *E. coli*. Three predicted PodJ interaction partners (PleC, CpaE, and PopA) exhibited mostly diffused pattern when expressed alone, but co-localized with PodJ at the cell poles when co-expressed (Figure 3A, 3B). Three other proteins (SpmX, FtsZ, and TipN) disrupted the PodJ localization pattern when co-expressed with them in *E. coli* (Figure S3C), suggesting they could serve as a negative regulator of PodJ localization. We were unable to detect any direct interactions between PodJ and the following new cell pole signaling proteins: DivL, DivK, CckA, ParA, ParB, and PleD (Figure S3D, Figure 3B). These results support a model of PodJ as a scaffold protein that directly recruits at least three client proteins: PleC, CpaE and PopA.

Amongst these proteins, the positioning of PleC at the new cell pole is critical for activation of the CtrA signaling pathway and generation of a CtrA signaling gradient (Chen et al., 2011; Matroule et al., 2004). Two regions of PodJ which contribute additively to the localization of PleC: the C-terminal peptidoglycan binding domain (residues 921-974) and residues 589-639 (Curtis et al., 2012; Lawler et al., 2006). Through the *E. coli* heterologous co-expression assay (Figure S4) we observed that PleC could co-localize robustly with a PodJ variant lacking the C-terminal periplasmic region (PodJΔ703-974, Figure 3C). Deletion of either the N-terminal (PodJΔ471-588) or the C-terminal (PodJ Δ589-642) disordered region resulted in a loss of PleC co-localization in *E. coli* (Figure 3C). These results suggest that the entire disordered region of PodJ serves as a binding site for PleC and may be involved in weak multivalent interactions with this domain. Moreover, we demonstrated that *C. crescentus* cells that express PodJΔPSE as a sole copy display a diffuse PleC subcellular localization pattern in a

185 manner similar to the Δ*podJ* strain (Figure 3D). We next tested if the negatively charged
186 disordered region could be substituted with other disordered proteins, by replacing PodJ's PSE
187 domain with PopZ's disordered PED-rich domain. A similar diffuse pattern of PleC was
188 observed in *E. coli* when we swapped the PodJ PSE-rich disordered region with the disordered
189 PED-rich region from PopZ(Holmes et al., 2016) (Figure 3C). Therefore, our results emphasized
190 the PSE domain likely presents a specific site for recruitment of PleC client proteins.
191 We fluorescently labeled PodJ_PSE domain with a BODIPY dye and measured binding
192 via a fluorescence polarization assay by mixing 16 μM of PleC sensory domain with 100 nM of
193 BODIPY-PodJ_PSE. As shown in Figure 3E, PodJ_PSE bound selectively to PleC, however did
194 not bind to other signaling proteins (e.g. CckA and DivL) that co-localize at the new cell pole.
195 In summary, by integrating our studies together with previous work from PopZ (Holmes et al.,
196 2016), DivL(Mann and Shapiro, 2018; Tsokos et al., 2011), and CckA (Biondi et al., 2006), we
197 have mapped out a localization dependency hierarchy that implicates two scaffolds, PodJ and
198 PopZ, as nucleating factors for new cell pole assembly (Figure 3F).
199 ***PodJ nucleates PopZ assembly at the new cell pole in C. crescentus***
200 PopZ plays a critical role in the predivisional cell polarity establishment by switching from a
201 monopolar to bipolar localization (Bowman et al., 2010; Ptacin et al., 2014) and recruiting core
202 CtrA regulatory proteins: DivL, CckA, and ChpT (Holmes et al., 2016). We tested if PopZ
203 accumulation at the new cell pole was PodJ dependent in *C. crescentus*. We observed that in the
204 Δ*podJ* strain, there was a 4-fold reduction in the fraction of mCherry-PopZ signal at the new cell
205 pole versus wild-type strains (Figure 4A, 4B). Notably, robust PopZ accumulation at the new cell
206 pole could be rescued when sfGFP-*podJ* was expressed from the chromosomal xylose locus
207 (Figure 4A-D). To examine the distribution of mcherry-PopZ during the cell cycle, we

208 performed a series of time-lapse microscopy experiments starting with a synchronized
209 population of swarmer cells (Figure 4C). Images were acquired every one minute and
210 kymographs were constructed to show the fluorescence intensity along the cell body over time.
211 In wild-type cells, robust mCherry-PopZ foci accumulates at the new cell pole approximately 40
212 minutes post-synchrony (Figure 4C, movie 2). However, in a Δ*podJ* strain the vast majority of
213 cells (90%, Figure 4D) proceed through cell division without accumulating any detectable PopZ
214 at the new cell pole (Figure 4C, movie 3). Quantitative analyses in Figure 4D show that the
215 proportion of the cells containing bipolar PopZ reaches the highest of ~80% at 105-minute post-
216 synchrony for wild-type and *podJ*$^{+}$ cells, comparing to the highest of 10% in Δ*podJ* cells.
217 Collectively, these results show that PodJ is required for robust PopZ accumulation at the new
218 cell pole in *C. crescentus*. A subpopulation that does accumulate at the new cell pole implicates
219 redundant factors such as TipN(Laloux and Jacobs-Wagner, 2013) and ZitP(Berge et al., 2016)
220 assist in PopZ recruitment at the new cell pole.

221 ***In the absence of PodJ, the cell polarity axis is randomized***

222 In wild-type cells, PopZ accumulation at the new cell pole prior to cell division ensures that
223 swarmer daughter cell inherit a PopZ signaling complex that maintains CtrA activation and
224 prevents chromosome replication. In contrast, within the Δ*podJ* strain, the disability of PopZ to
225 accumulate at the new cell pole led to 86% (82 out of 95 cells) of swarmer daughter cells void of
226 PopZ (Figure 4E, Figure S4). In these cells, nascent PopZ is accumulated as monopolar focus
227 approximately 60 minutes after cell division (Figure 4C). In *C. crescentus* Δ*podJ* strain, time-
228 lapse analysis showed that in 91% of cells, PopZ accumulates at the same pole as in the wild-
229 type strain (Figure 4F). However, in the other 9% of cells, PopZ accumulates at the opposite cell
230 pole, disrupting the inherited cell polarity axis. These results indicate that PodJ is required to

231 strictly maintain the inherited polarity axis for the newborn swarmer cells, and that other possible
232 polarity factors (*e.g.*, SpmX or ParB) likely facilitate proper subcellular recruitment of nascent
233 PopZ.

234 ***CtrA pathway activation requires new cell pole assembly***

235 Establishment of the new cell pole signaling complex is required for activation of the
236 CtrA signaling pathway and repression of chromosome replication. Previous studies revealed
237 that several new cell pole signaling proteins that promote CtrA phosphorylation (DivL, CckA,
238 and PleC) displayed reduced accumulation at the new cell pole in the ΔPodJ strain(Curtis et al.,
239 2012). Here we have shown that PodJ is a direct binding partner for PleC (Figure 3) and PopZ
240 (Figure 4), which recruits the DivL/CckA complex(Holmes et al., 2016). To investigate the
241 impact of new cell pole signaling hub disruption from the ΔPodJ strain, we examined the impact
242 upon the CtrA signaling pathway activation by flow cytometry analysis of exponentially growing
243 *WT* and Δ*podJ* cells stained with the nucleic acid dye SYTOX Green. Phosphorylated CtrA
244 serves as a direct inhibitor of chromosome replication resulting in a tightly regulated cell
245 population that contains either one or two chromosomes. A lower 1N:2N chromosome ratio was
246 observed in Δ*podJ* cultures compared with *WT*, as well as a substantial increase in cells with
247 three or more chromosomes (Figure 4G). These results indicate that PodJ's scaffolding functions
248 at the new cell pole promote CtrA signaling pathway activation.
249

PopZ binds directly to coiled-coil region 4-6 of PodJ

To determine if PopZ and PodJ interact directly, we heterologously expressed fluorescent protein fusions of PodJ and PopZ in *E. coli*. As shown in Figure 5A and 5B, mCherry-PopZ accumulates at a single cell pole when it is expressed alone, while PopZ co-localizes in a bipolar pattern when co-expressed with YFP-PodJ. To determine the PopZ binding site within PodJ, we screened the capability of PopZ to bind to the library of PodJ domain deletion variants through co-expression in *E. coli* (Figure 5C, Figure S2). We used the following screening criteria to characterize PopZ interaction with the PodJ variants: (a) the two proteins are 100% co-localized and (b) the monopolar localization pattern of PopZ is changed after co-expression. We found that deletion of the C-terminal periplasmic domain or the intrinsically disordered PSE domain in PodJ did not disrupt the PodJ-PopZ interaction (Figure 5C, S2). In contrast, deletion of its CC4-6 domains disrupted PopZ co-localization with PodJ. We then expressed YFP-CC4-6 alone and observed that it was dispersed through the cytoplasm in *E. coli*. However, mCherry-PopZ was able to recruit it to the cell pole when co-expressed them in *E. coli.* These data indicate that coiled-coil 4-6 in PodJ functions as a PopZ recruitment site (Figure 5C).

To confirm this PopZ-PodJ protein-protein interaction is direct, we purified the PodJ_CC4-6 protein with a cysteine incorporated after the hexahistidine purification tag and fluorescently labeled it as with PodJ_PSE. A fluorescence polarization assay was employed to detect a binding interaction between PodJ and PopZ by mixing 16 μM PopZ together with 100 nM BODIPY-PodJ_CC4-6, using the same amount of BODIPY-PodJ_PSE as a control. As shown in Figure 5D, PopZ bound to PodJ_CC4-6, but did not bind to PodJ_PSE. Taken together, the *E. coli* heterologous expression assays and *in vitro* biochemical assays show that coiled-coil 4-6 region of PodJ is the site of interaction with PopZ (Figure 5E). Moreover, we propose this

PodJ-PopZ interaction plays a critical role in maturation of the new cell pole signaling hub (Figure 4A-F) and transcriptional regulation of PodJ(Crymes et al., 1999) coordinates this event with chromosomal replication (Figure 5E).

SpmX is a negative regulator of PodJ accumulation at the cell poles.

Our PodJ overexpression experiments (Figure 1D) and *E. coli* reconstitution experiments (Figure 2C) suggest that PodJ has an affinity for both cell poles. But how does PodJ exclusively bind and recognize the new cell pole in *C. crescentus*? Eukaryotic cell polarity networks are characterized by inhibitory regulatory interactions between the asymmetrically partitioned complexes to ensure robust cell polarization (Chau et al., 2012). Based upon these eukaryotic polarity networks, we hypothesized that proteins that reside at the old cell pole (*e.g.*, SpmX or DivJ) might play a role as a negative regulator of PodJ subcellular accumulation (Chau et al., 2012). We found that overexpression of SpmX resulted in a significant reduction of PodJ at the cell poles compared to that in wild-type cells (Figure 6A, 6C). In contrast, sfGFP-PodJ accumulated at all cell poles including constricted mid-cell curved sites in Δ*spmX* mutant strains (Figure 6B, 6C). These results suggest that SpmX is a negative regulator of PodJ accumulation at the cell poles either directly or indirectly.

We further examined if SpmX could disrupt PodJ subcellular accumulation at the cell poles when co-expressed in *E. coli* (Figure 6D). Consistent with previous studies (Holmes et al., 2016; Perez et al., 2017), SpmX expression alone is diffuse in *E. coli*. PodJ itself accumulates at the cell poles however co-expression of SpmX and PodJ together resulted in dispersion of the PodJ (Figure 6D). These results suggested that PodJ and SpmX interact directly and that dispersal of PodJ from the cell poles depends on the increase of SpmX protein level, consistent

295 with the up-regulation of SpmX at the G1 transition phase in *C. crescentus* (Radhakrishnan et al.,
296 2008; Schrader et al., 2016) (Figure 1A).

297 ***SpmX interacts with the CC4-6 and PSE-rich domains of PodJ***

298 To determine the SpmX interaction domain, we co-expressed a library of PodJ domain deletions
299 in *E. coli* with a SpmX variant lacking the transmembrane domains, hereafter called SpmX'.
300 While full-length SpmX is disperse throughout the cytoplasm, SpmX' accumulates at both cell
301 poles. We observed that co-expression of PodJ with SpmX' resulted in PodJΔCC4-6 foci
302 accumulation away from the cell poles. When the PodJ CC4-6 variant is expressed by itself in *E.*
303 *coli* it was diffuse (Figure 6E, 6F), however SpmX' is capable of recruiting PodJ CC4-6 to the
304 cell poles. This result indicates that SpmX' binds directly to coiled-coil 4-6 region of PodJ. We
305 then more closely examined the role of PodJ's PSE domain in the PodJ-SpmX interaction. Upon
306 SpmX co-expression with PodJΔPSE we observed that the two proteins co-localized at the cell
307 poles without any observed dispersal from the cell poles. We also observed that expression of the
308 PSE-rich domain by itself could disperse SpmX from the cell poles in *E. coli*. These data indicate
309 that SpmX dependent dispersion of PodJ also requires the PSE domains. As the CC4-6 and PSE
310 domains are adjacent to one another they may work collectively to regulate the PodJ-SpmX
311 interaction.

312 To confirm PodJ and SpmX interact directly, we purified SpmX', and employed the
313 fluorescence polarization assay to detect the interaction between SpmX' and the BODIPY-
314 PodJ_CC4-6 or BODIPY-PodJ_PSE. As shown in Figure 6G, SpmX' interacted with both
315 BODIPY-PodJ_CC4-6 and BODIPY-PodJ_PSE. Interestingly, the consequences of these two
316 binding interactions are distinct: SpmX binding to CC4-6 region results in co-localization, while
317 SpmX binding to the PSE-domain results in PodJ and SpmX dispersal from the cell poles.

PodJ interactions with PopZ and SpmX are required for robust cell polarity

Our experiments suggest a 3-node protein-protein interaction circuit in which PodJ promotes PopZ new cell pole accumulation (Figure 4), PopZ promotes SpmX subcellular accumulation(Perez et al., 2017), and SpmX negatively regulates PodJ subcellular accumulation (Figure 6). We introduced PodJ variants as a sole copy into *C. crescentus* that would individually disrupt the proposed regulatory interactions and evaluated their impact upon *C. crescentus* cell polarity: PodJΔperi, PodJΔCC4-6 and PodJΔPSE. When sfGFP-PodJΔPSE is expressed as a sole copy in *C. crescentus*, we observed that sfGFP-PodJΔPSE and mCherry-PopZ accumulates at both cell poles in predivisional cells (Figure 7A). This indicates the PSE domain in PodJ, the site of PodJ-SpmX interaction, is critical for PodJ to be excluded from the old cell pole. When sfGFP-PodJΔCC4-6 is expressed as a sole copy in *C. crescentus*, we found that PopZ-mCherry is poorly localized at the new cell pole (Figure 7A), similar to the observation that was found in Δ*podJ* (Figure 4B). Therefore, deletion of CC4-6 disrupts polarity through loss of PopZ recruitment at the new cell pole. In contrast, sfGFP-PodJΔperi construct mirrors wild-type like cell polarity (Figure 7A) as it contains critical regulatory interactions with PopZ and SpmX.

To our surprise, we observed that sfGFP-PodJΔCC4-6 is secreted from the stalked pole in wild-type cells (Figure S7, Figure 7A). However, this abnormal phenotype can be restored by deleting *spmX* (Figure S7). Moreover, besides dispersal of intracellular PodJ, overexpression of SpmX also resulted in secretion of PodJ foci from the cell (Figure 6A, Movie S4), indicating SpmX plays a role in secretion of PodJ. Similar secretion phenotype was observed when expression sfGFP-PodJ after deletion of PopZ (Figure S7), suggesting that PopZ anchors PodJ in the cytoplasm and prevents this abnormal secretion process. To exclude the possibility that PodJ is excreted due to cell lysis, we confirmed sfGFP-PodJ by western blot analyses of the media

341 supernatants with anti-GFP antibody, using the intracellular CtrA protein as a negative control
342 (Figure S7). These results collectively suggest that SpmX plays a negative regulatory role in
343 dispersing PodJ from the old cell pole, a function that we propose is critical for the new-to-old
344 cell pole remodeling that triggers swarmer-to-stalk cell differentiation (Figure 7B).
345
346 **Discussion**
347 Here we have shown that the protein-protein interactions between three scaffolding proteins
348 function together as a circuit to establish and maintain polarity in *C. crescentus.* Using a
349 synthetic biology reconstitution approach, we have identified the localization hierarchy at the
350 new cell pole by demonstrating that PodJ recruits three client proteins (PleC, CpaE, PopA), and
351 the central organizing scaffold PopZ. In turn, this allows PopZ to recruit its direct binding
352 partners (DivL, CckA) to the new cell pole (Figure 3F) (Holmes et al., 2016). Thus the PodJ
353 scaffold promotes the colocalization of PleC together with the PopZ/DivL/CckA signaling
354 complex to promote CtrA pathway activation (Figure 4G). To trigger asymmetric accumulation
355 of PodJ, our studies have also revealed that the old cell pole scaffold SpmX promotes localized
356 foci disassembly and an unexpected stalked pole specific secretion process (Figure 6-7). Taken
357 together we propose that this scaffold network topology composed of both positive feedback and
358 negative regulations between signaling hubs promotes robust cell polarization (Figure 7).
359 ***PodJ serves as a central node in the new cell pole signaling hub localization hierarchy***
360 Prior to this study it was known that several factors accumulate at the new cell pole (Curtis and
361 Brun, 2010; Lasker et al., 2016), however the localization dependency within this new cell pole
362 signaling hub was unclear. We confirmed that three protein-protein interactions with the client
363 proteins CpaE, PleC and PopA were direct. Most critically, we discovered a direct PodJ-PopZ

364 interaction that further triggers accumulation of PopZ binding proteins (DivL and CckA). In the
365 absence of PodJ, the PopZ scaffold still can accumulates at the new cell pole in a fraction of cells
366 (Figure 4), consistent with contribution of other redundant factors such as ZitP(Berge et al.,
367 2016) and TipN(Laloux and Jacobs-Wagner, 2013). These studies indicate that the PodJ
368 scaffold serves as a central organizer of the new cell pole development (Figure 3F). Key
369 questions remain as to the mechanism of how this nucleating factor targets the cell poles? Our
370 studies indicate that oligomerization of PodJ (Figure 2) may allow PodJ to recognize micron
371 sized curvature differences (Huang and Ramamurthi, 2010) or interact with shared cell wall
372 components between *C. crescentus* and *E. coli* such as the Tol-Pal membrane integrity complex
373 (Yeh et al., 2010), pili and flagellar assemblies.
374
375 ***SpmX prevents symmetric PodJ localization***
376 A key aspect of eukaryotic cell polarity circuits are regulatory interactions between partitioned
377 complexes(Chau et al., 2012). Our studies have revealed that SpmX is a novel negative regulator
378 of PodJ localization. Deletion of SpmX results in accumulation of PodJ at all highly curved
379 regions of the cell (Figure 6A) while overexpression of SpmX results in dispersion of PodJ from
380 the cell poles and an unexpected localized secretion of PodJ at the stalked cell pole (Figure 6A,
381 Figure S7(Grangeon et al., 2015)). We propose that this local PodJ dispersal functions may play
382 a role in compositional remodeling of the PodJ-rich signaling hub into a SpmX-rich signaling
383 hub that occurs in the swarmer-to-stalked cell differentiation (Figure 7B).
384 PodJ domain analysis indicates that SpmX binds to two PodJ domains: CC4-6 and the
385 instrically disordered PSE-rich domain. The biophysical mechanism of this foci disassembly
386 process remains unclear, and one possible model is that PodJ-SpmX complex forms small

387 oligomers incapable of cell pole recognition. We speculate that the SpmX-PodJ regulatory
388 interactions may share broad mechanistic similarities with the MipZ-FtsZ (Thanbichler and
389 Shapiro, 2006) and (MinD-FtsZ) (Park et al., 2018) interactions that prevent FtsZ accumulation
390 at the cell poles and direct FtsZ to the mid-plane. However, extensive future *in vitro* studies will
391 be needed to fully understand this dispersal mechanism. As well, we anticipate that SpmX likely
392 mediates other cell pole remodeling mechanisms indirectly which will require future genetic
393 studies to identify new regulatory partners and interactions. It also remains to be seen if co-
394 localization of PodJ, the ClpXP adaptor protein PopA and ClpXP promote the final stages of
395 $PodJ_S$ proteolysis at the old cell pole to promote asymmetric localization.
396
397 ***Cell polarity is achieved though polarity circuits with common network topology throughout***
398 ***all kingdoms of life***
399 The PopZ-SpmX-PodJ polarity circuit is conserved within a subset of α-proteobacteria, and
400 recent studies of have revealed genetic interactions between PodJ and PopZ in *Agrobacterium*
401 *tumefaciens* (Anderson-Furgeson et al., 2016; Grangeon et al., 2015), however the subcellular
402 localization pattern of these proteins diverges from that observed in *C. crescentus* (Anderson-
403 Furgeson et al., 2016; Ehrle et al., 2017; Grangeon et al., 2015; Howell et al., 2017). In *A.*
404 *tumefaciens*, the polarity is inverted compare to *C. crescentus* as PopZ residues exclusively at the
405 new cell pole and PodJ occupies the old cell pole (Grangeon et al., 2015). Moreover, a second
406 subset of α-proteobacteria species encode the PopZ scaffolding protein and the PleC and CckA
407 histidine kinases, however their genomes contain no clear homologs of the PodJ or SpmX
408 scaffolding proteins. These variations in conservation suggest that that the PopZ-SpmX-PodJ
409 polarity network may have been re-wired to include new regulatory interactions and new

410 regulators to support diverse modes of bacterial cell development observed throughout α-
411 proteobacteria (Ettema and Andersson, 2009).

412 More broadly, polarity networks are remarkably diverse at the biomolecular level and are
413 utilized throughout all kingdoms of life. *C. crescentus* orchestrates cell polarity through a
414 network architecture that contains positive feedback through formation self-assembled
415 scaffolding proteins. With positive feedback alone, PodJ self-assembles or binds to cell pole
416 binding sites nearly equally well at each cell pole. In this study we have critically examined the
417 inter-relationships between three scaffolds that promote *C. crescentus* cell polarity. Based upon
418 these studies we propose a model that compositional control of the new and old cell pole
419 signaling hubs is promoted by local disassembly of PodJ at the old cell pole by a PodJ foci
420 inhibitor protein SpmX (Figure 7B). Remarkably, this network topology of positive feedback
421 coupled with inhibition is similar to minimal polarity circuit architectures identified using a
422 synthetic biology approach in yeast (Chau et al., 2012). This synthetic biology approach
423 characterizing several network architectures suggested that mutual inhibition networks yielded
424 the most robust cell polarization (Chau et al., 2012). Therefore, we anticipate future research will
425 identify several negative regulatory interactions between the new and old cell pole signaling
426 hubs to ensure robust *C. crescentus* cell polarization.

427

428 **Figure Captions**

429 **Figure 1: The scaffolding protein PodJ recognizes the new pole and is involved in cell**
430 **polarity establishment.** (A) Schematic of cell polarity establishment and cell cycle regulation in
431 *Caulobacter crescentus*. Swarmer cells differentiate into stalked cells, which is correlated with
432 cell pole remodeling of a PodJ-rich signaling hub (green) into a SpmX-rich signaling hub (red).

433 In stalked cells, after initiation of replication a PodJ-rich signaling hub accumulates at the new
434 cell pole. Cell division results in a swarmer cell that involved unequal inheritance of a PodJ-rich
435 signaling hub in swarmer cells and a SpmX-rich signaling hub in stalked cells. (B) Two key
436 cell-cycle regulators, CtrA and DnaA, co-regulate the initiation of replication and the
437 transcription of PodJ and a PodJ specific protease PerP (C and D) Time-lapse microscopy
438 analyses show PodJ accumulates at the new cell pole during the cell cycle. Kymographs of
439 sfGFP-PodJ signal along the cell length over time after the synchronization of WSC1201
440 swarmer cells, images were acquired every 2 min. (E) Constitutive overnight PodJ
441 overexpression (0.3% xylose) causes formation of ectopic cell poles that are co-localized with
442 PodJ foci. Two representative cells are shown. All bars, 2 μm.
443
444 **Figure 2: PodJ is a self-assembled protein, whose monopolar accumulation is dependent**
445 **upon PodJ and SpmX.** (A) PodJ domain organization predicted by HHpred and adapted from
446 previous studies(Curtis et al., 2012; Lawler et al., 2006) The coiled-coil rich region was analyzed
447 by PCOILS and modeled with MODELLER. The probability of intrinsic disorder over the
448 primary sequence of PodJ (red line), represented as the average scores from four disorder
449 prediction algorithms: Meta disorder MD2, SPOT, Cspritz*2, and MFDp2. (B) PodJ
450 accumulation as a concentrated focus in *C. crescentus* cells is independent of TipN, PleC, PopZ
451 and SpmX. However, PodJ monopolar subcellular accumulation is dependent upon the PopZ
452 and SpmX scaffolds. (C) Subcellular localization of PodJ when heterologously expressed YFP-
453 PodJ in *E. coli*. (D) Heterologous expression of YFP-PodJ variants in *E. coli* reveals that the N-
454 terminal coiled-coil region 1-3 is critical for accumulation of PodJ at the cell poles. (E) The
455 signal of YFP-PodJ along the cell length was plotted for the cells shown in Figure 2D. All of the

456 data was normalized with the highest intensity in each strain setting as 100%. (F) Purified
457 PodJ(1-635) was analyzed *in vitro* via native gel analysis. The protein is subjected to
458 nondenaturing gel electrophoresis at 4°C and subsequently stained with Coomassie blue stain.
459 Four distinct bands indicate PodJ oligomers larger 480 kDa. (G) Analytical size exclusion
460 chromatography was used to measure the apparent molecular mass of purified PodJ(1-635)
461 (black line), by plotting absorbance at 215 nm versus elution volume. The indicated molecular
462 masses of each peak were determined by comparison to the elution volume of protein standards
463 (grey lines). A representative trace is shown from three independent replicates.
464
465 **Figure 3: PodJ is a central organizer of the new cell pole signaling hub.** The interactions
466 between PodJ and binding partners were evaluated through heterologous co-expression in *E. coli*.
467 (A) YFP-PodJ exhibits selective recruitment roles for the *C. crescentus* new cell pole proteins
468 that include PleC, PopA and CpaE. (B) The polar recruitment ability by PodJ was calculated and
469 normalized as a relative localization index. (C) Co-expression of PodJ variants together with
470 PleC reveals that the intrinsically disordered PSE-rich domain is necessary for PleC recruitment
471 to the cell pole in *E. coli*. (D) Expression of PodJ variants as a sole-copy in *C. crescentus*
472 revealed that the PSE-rich domain is required for PleC accumulation at the new cell poles. (E)
473 Fluorescence polarization binding assay confirms PodJ directly interaction with PleC. 100 nM
474 BODIPY dye labeled PodJ_PSE mixed with the following new cell pole proteins at 10 μM
475 PopZ, PleC, CckA and DivL. PodJ_PSE specifically binds to PleC. (G) New cell pole
476 localization hierarchy based upon these studies indicate that PodJ is a central organizer in
477 addition to PopZ(Holmes et al., 2016) for the new cell pole signaling hub. Interactions identified
478 in this study (red), and those discovered previously by Holmes et al. (blue)(Holmes et al., 2016).

Figure 4: **PodJ nucleates PopZ assembly at the new cell pole and is required for robust inheritance of PopZ in daughter swarmer cells.** (A) mCherry-PopZ localization in predivisional cells in the wild-type (bipolar) versus the *podJ* deletion *C. crescentus* (monopolar). Bars, 2 μm. (B) Population analysis reveals a substantial reduction of PopZ abundance at the new cell pole of Δ*podJ* predivisional cells. Cell poles (new or old) were distinguished and orientated manually by observation of a stalk. The signal intensity was normalized with the highest value as 100% in each strain. (C) Kymograph analyses of mCherry-PopZ signal over the time after the synchronization of WT, Δ*podJ* and *podJ* complementary cells. Vanillate (50 mM) for mChy-PopZ induction and xylose (0.03%) for sfGFP-PodJ induction were added at 1 hr prior to synchronization of the cell culture. Images were acquired every 1 min. One of three representative cells were shown for each strain. The results indicate that PopZ fails to robustly accumulate at the new cell poles prior to cell division in Δ*podJ* strain. (D) Quantification of the percentage of cells that display detectable bipolar PopZ after cell synchronization. Time course analyses were performed within 135 mins in PYE medium for WT, □*podJ* and *podJ* complementary cells (more than 130 cells were calculated for each point). Robust PopZ assembly at the new cell pole is dependent upon PodJ. (E and F) Failure to localize mcherry-PopZ to the new cell pole in Δ*podJ* results in ~80% population of swarmer cells that fail to inherit PopZ. Within a subpopulation of swarmer cells (9% of cells), nascent PopZ accumulates at the incorrect cell pole switching the inherited polarity axis. A total of 40 cells were tracked by time-lapse analyses. (G) Flow cytometry analysis of wild-type versus Δ*podJ* strains. When podJ is deleted from cells (red line), cells display a decrease in 1N and 2N cells that is accompanied with an increase in 3N and 4N cells.

Figure 5: **PopZ binds directly to the coiled-coil 4-6 region of PodJ. (A)** Heterologous expression of YFP-PodJ and mcherry-PopZ in *E. coli*. Co-expression with PodJ causes bipolar PopZ accumulation in *E. coli*. (B) Mean protein intensity of YFP-PodJ and mcherry-PopZ versus cell length (n=370). The signal intensity was normalized with the highest value as 100% in each strain. (C) Co-expression of PodJ variants together with PopZ in *E. coli* reveals that the coiled-coil 4-6 region in PodJ is necessary for the interaction with PopZ. (D) Fluorescence polarization binding assay of the BODIPY dye labeled PodJ_PSE or PodJ_CC4-6 mixed with 10 μM PopZ, using BSA as a negative control. PopZ binds specifically to the CC4-6 domain of PodJ, however does not bind to its PSE-rich domain (E) Model for PodJ serving as a new cell pole development signal that triggers polarity establishment upon the initiation of replication, through its cell-cycle coordinated expression and specific interaction with the PopZ scaffold. All bars, 2 μm.

Figure 6: **SpmX is a negative regulator for cell pole accumulation of PodJ.** (A) SpmX directly or indirectly regulates PodJ subcellular localization in *C. crescentus*. Overexpression of SpmX results in a reduction of cell pole localized PodJ and secretion of PodJ from cells. (B) In the absence of SpmX, PodJ accumulates at all poles in *C. crescentus*. (C) Quantitative analysis of PodJ localization in *C. crescentus* predivisional cells in wild-type, Δ*spmX* and SpmX overexpression strains. (D) Heterologous expression of YFP-PodJ alone results in bipolar PodJ accumulation, while expression of SpmX-mcherry alone is disperse in *E. coli*. (E) Co-expression of PodJ together with SpmX causes PodJ to disperse from the cell poles in *E. coli*. All bars, 2 μm. (F) Co-expression of PodJ variants together with a SpmX variant lacking the transmembrane domain (SpmX'). These analyses indicate that SpmX's dispersal of PodJ requires the PSE and

525 CC4-6 domains of PodJ. (G) I*n vitro* fluorescence polarization assays screening the binding
526 interactions between SpmX and Bodipy labeled PodJ-PSE domain and PodJ-CC4-6 domains.
527
528 Figure 7: **A network of protein-protein regulatory interactions enable polarity**
529 **establishment in *C. crescentus***
530 (A) A polarity circuit in which PodJ promotes PopZ new cell pole localization, PopZ promotes
531 SpmX accumulation at the cell poles, and SpmX negatively regulates PodJ subcellular
532 localization at the cell poles Expression of PodJ variants and PopZ as the sole copy in *C.*
533 *crescentus*. The cytoplasmic domain of PodJ, containing both CC4-6 and the PSE-rich domain,
534 supports bipolar localization of PopZ and new cell pole localization of PopZ. In contrast,
535 expression of PodJΔCC4-6 results in predivisional cells that fails to accumulate PopZ at the new
536 cell pole. Removal of the domain that is required for SpmX to disperse PodJ from the cell poles,
537 PodJΔPSE, results in PodJ accumulation at both cell poles in *C. crescentus*. These results
538 indicate that the regulatory protein-protein interaction between PodJ, PopZ and SpmX are
539 required for robust cell polarity of *C. crescentus* predivisional cells. **(B)** SpmX functions as a
540 local negative regulator of PodJ accumulation at the old cell pole. **(C)** The establishment of the
541 compositionally distinct new and old cell poles is driven by a network of scaffolding proteins
542 that combines positive feedback together with inhibition.
543 References
544 Aakre, C.D., and Laub, M.T. (2012). Asymmetric cell division: a persistent issue?
545 Developmental cell *22*, 235-236.
546
547 Anderson-Furgeson, J.C., Zupan, J.R., Grangeon, R., and Zambryski, P.C. (2016). Loss of PodJ
548 in Agrobacterium tumefaciens Leads to Ectopic Polar Growth, Branching, and Reduced Cell
549 Division. Journal of bacteriology *198*, 1883-1891.
550

551 Ardissone, S., Fumeaux, C., Berge, M., Beaussart, A., Theraulaz, L., Radhakrishnan, S.K.,
552 Dufrene, Y.F., and Viollier, P.H. (2014). Cell cycle constraints on capsulation and bacteriophage
553 susceptibility. Elife *3*.
554
555 Berge, M., Campagne, S., Mignolet, J., Holden, S., Theraulaz, L., Manley, S., Allain, F.H., and
556 Viollier, P.H. (2016). Modularity and determinants of a (bi-)polarization control system from
557 free-living and obligate intracellular bacteria. Elife *5*.
558
559 Bergé, M., and Viollier, P.H. (2018). End-in-Sight: Cell Polarization by the Polygamic Organizer
560 PopZ. Trends in Microbiology *26*, 363-375.
561
562 Biondi, E.G., Reisinger, S.J., Skerker, J.M., Arif, M., Perchuk, B.S., Ryan, K.R., and Laub, M.T.
563 (2006). Regulation of the bacterial cell cycle by an integrated genetic circuit. Nature *444*, 899-
564 904.
565
566 Bowman, G.R., Comolli, L.R., Gaietta, G.M., Fero, M., Hong, S.H., Jones, Y., Lee, J.H.,
567 Downing, K.H., Ellisman, M.H., McAdams, H.H.*, et al.* (2010). Caulobacter PopZ forms a polar
568 subdomain dictating sequential changes in pole composition and function. Molecular
569 Microbiology *76*, 173-189.
570
571 Bowman, G.R., Comolli, L.R., Zhu, J., Eckart, M., Koenig, M., Downing, K.H., Moerner, W.E.,
572 Earnest, T., and Shapiro, L. (2008). A polymeric protein anchors the chromosomal origin/ParB
573 complex at a bacterial cell pole. Cell *134*, 945-955.
574
575 Chau, A.H., Walter, J.M., Gerardin, J., Tang, C., and Lim, W.A. (2012). Designing synthetic
576 regulatory networks capable of self-organizing cell polarization. Cell *151*, 320-332.
577
578 Chen, J.C., Hottes, A.K., McAdams, H.H., McGrath, P.T., Viollier, P.H., and Shapiro, L. (2006).
579 Cytokinesis signals truncation of the PodJ polarity factor by a cell cycle-regulated protease. The
580 EMBO journal *25*, 377-386.
581
582 Chen, J.C., Viollier, P.H., and Shapiro, L. (2005). A membrane metalloprotease participates in
583 the sequential degradation of a Caulobacter polarity determinant. Mol Microbiol *55*, 1085-1103.
584
585 Chen, Y.E., Tropini, C., Jonas, K., Tsokos, C.G., Huang, K.C., and Laub, M.T. (2011). Spatial
586 gradient of protein phosphorylation underlies replicative asymmetry in a bacterium. Proc Natl
587 Acad Sci U S A *108*, 1052-1057.
588
589 Crymes, W.B., Jr., Zhang, D., and Ely, B. (1999). Regulation of podJ expression during the
590 Caulobacter crescentus cell cycle. Journal of bacteriology *181*, 3967-3973.
591
592 Curtis, P.D., and Brun, Y.V. (2010). Getting in the loop: regulation of development in
593 Caulobacter crescentus. Microbiol Mol Biol Rev *74*, 13-41.
594

595 Curtis, P.D., Quardokus, E.M., Lawler, M.L., Guo, X., Klein, D., Chen, J.C., Arnold, R.J., and
596 Brun, Y.V. (2012). The scaffolding and signalling functions of a localization factor impact polar
597 development. Mol Microbiol *84*, 712-735.
598
599 Ducret, A., Quardokus, E.M., and Brun, Y.V. (2016). MicrobeJ, a tool for high throughput
600 bacterial cell detection and quantitative analysis. Nature microbiology *1*, 16077.
601
602 Duerig, A., Abel, S., Folcher, M., Nicollier, M., Schwede, T., Amiot, N., Giese, B., and Jenal, U.
603 (2009). Second messenger-mediated spatiotemporal control of protein degradation regulates
604 bacterial cell cycle progression. Genes & development *23*, 93-104.
605
606 Ebersbach, G., Briegel, A., Jensen, G.J., and Jacobs-Wagner, C. (2008). A self-associating
607 protein critical for chromosome attachment, division, and polar organization in Caulobacter. Cell
608 *134*, 956-968.
609
610 Ehrle, H.M., Guidry, J.T., Iacovetto, R., Salisbury, A.K., Sandidge, D.J., and Bowman, G.R.
611 (2017). Polar Organizing Protein PopZ Is Required for Chromosome Segregation in
612 Agrobacterium tumefaciens. Journal of bacteriology *199*.
613
614 Ely, B. (1991). Genetics of Caulobacter crescentus. Methods Enzymol *204*, 372-384.
615 Ettema, T.J., and Andersson, S.G. (2009). The alpha-proteobacteria: the Darwin finches of the
616 bacterial world. Biology letters *5*, 429-432.
617
618 Evinger, M., and Agabian, N. (1977). Envelope-associated nucleoid from Caulobacter crescentus
619 stalked and swarmer cells. Journal of bacteriology *132*, 294-301.
620
621 Grangeon, R., Zupan, J.R., Anderson-Furgeson, J., and Zambryski, P.C. (2015). PopZ identifies
622 the new pole, and PodJ identifies the old pole during polar growth in Agrobacterium
623 tumefaciens. Proc Natl Acad Sci U S A *112*, 11666-11671.
624
625 Hanson, J., Yang, Y., Paliwal, K., and Zhou, Y. (2017). Improving protein disorder prediction by
626 deep bidirectional long short-term memory recurrent neural networks. Bioinformatics (Oxford,
627 England) *33*, 685-692.
628
629 Hardy, G.G., Allen, R.C., Toh, E., Long, M., Brown, P.J., Cole-Tobian, J.L., and Brun, Y.V.
630 (2010). A localized multimeric anchor attaches the Caulobacter holdfast to the cell pole.
631 Molecular microbiology *76*, 409-427.
632
633 Hinz, A.J., Larson, D.E., Smith, C.S., and Brun, Y.V. (2003). The Caulobacter crescentus polar
634 organelle development protein PodJ is differentially localized and is required for polar targeting
635 of the PleC development regulator. Mol Microbiol *47*, 929-941.
636
637 Holmes, J.A., Follett, S.E., Wang, H., Meadows, C.P., Varga, K., and Bowman, G.R. (2016).
638 Caulobacter PopZ forms an intrinsically disordered hub in organizing bacterial cell poles. Proc
639 Natl Acad Sci U S A *113*, 12490-12495.

640 Holtzendorff, J., Hung, D., Brende, P., Reisenauer, A., Viollier, P.H., McAdams, H.H., and
641 Shapiro, L. (2004). Oscillating global regulators control the genetic circuit driving a bacterial cell
642 cycle. Science (New York, NY) *304*, 983-987.
643
644 Howell, M., Aliashkevich, A., Salisbury, A.K., Cava, F., Bowman, G.R., and Brown, P.J.B.
645 (2017). Absence of the Polar Organizing Protein PopZ Results in Reduced and Asymmetric Cell
646 Division in Agrobacterium tumefaciens. Journal of bacteriology *199*.
647
648 Huang, K.C., and Ramamurthi, K.S. (2010). Macromolecules that prefer their membranes curvy.
649 Molecular Microbiology *76*, 822-832.
650
651 Huitema, E., Pritchard, S., Matteson, D., Radhakrishnan, S.K., and Viollier, P.H. (2006).
652 Bacterial birth scar proteins mark future flagellum assembly site. Cell *124*, 1025-1037.
653
654 Kozlowski, L.P., and Bujnicki, J.M. (2012). MetaDisorder: a meta-server for the prediction of
655 intrinsic disorder in proteins. BMC bioinformatics *13*, 111.
656
657 Laloux, G., and Jacobs-Wagner, C. (2013). Spatiotemporal control of PopZ localization through
658 cell cycle-coupled multimerization. The Journal of cell biology *201*, 827-841.
659
660 Lam, H., Schofield, W.B., and Jacobs-Wagner, C. (2006). A landmark protein essential for
661 establishing and perpetuating the polarity of a bacterial cell. Cell *124*, 1011-1023.
662
663 Lasker, K., Mann, T.H., and Shapiro, L. (2016). An intracellular compass spatially coordinates
664 cell cycle modules in Caulobacter crescentus. Current opinion in microbiology *33*, 131-139.
665
666 Laub, M.T., Chen, S.L., Shapiro, L., and McAdams, H.H. (2002). Genes directly controlled by
667 CtrA, a master regulator of the Caulobacter cell cycle. Proceedings of the National Academy of
668 Sciences of the United States of America *99*, 4632-4637.
669
670 Lawaree, E., Gillet, S., Louis, G., Tilquin, F., Le Blastier, S., Cambier, P., and Matroule, J.Y.
671 (2016). Caulobacter crescentus intrinsic dimorphism provides a prompt bimodal response to
672 copper stress. Nature microbiology *1*, 16098.
673
674 Lawler, M.L., Larson, D.E., Hinz, A.J., Klein, D., and Brun, Y.V. (2006). Dissection of
675 functional domains of the polar localization factor PodJ in Caulobacter crescentus. Mol
676 Microbiol *59*, 301-316.
677
678 Li, F., He, X., Ye, D., Lin, Y., Yu, H., Yao, C., Huang, L., Zhang, J., Wang, F., and Xu, S.
679 (2015). NADP(+)-IDH Mutations Promote Hypersuccinylation that Impairs Mitochondria
680 Respiration and Induces Apoptosis Resistance. Molecular Cell *60*, 661.
681
682 Lindner, A.B., Madden, R., Demarez, A., Stewart, E.J., and Taddei, F. (2008). Asymmetric
683 segregation of protein aggregates is associated with cellular aging and rejuvenation. Proc Natl
684 Acad Sci U S A *105*, 3076-3081.
685

686 Mann, T.H., and Shapiro, L. (2018). Integration of cell cycle signals by multi-PAS domain
687 kinases. Proc Natl Acad Sci U S A *115*, E7166-e7173.
688
689 Matroule, J.Y., Lam, H., Burnette, D.T., and Jacobs-Wagner, C. (2004). Cytokinesis monitoring
690 during development; rapid pole-to-pole shuttling of a signaling protein by localized kinase and
691 phosphatase in Caulobacter. Cell *118*, 579-590.
692
693 McAdams, H.H., and Shapiro, L. (2009). System-level design of bacterial cell cycle control.
694 FEBS letters *583*, 3984-3991.
695
696 Mera, P.E., Kalogeraki, V.S., and Shapiro, L. (2014). Replication initiator DnaA binds at the
697 Caulobacter centromere and enables chromosome segregation. Proceedings of the National
698 Academy of Sciences of the United States of America *111*, 16100-16105.
699
700 Ozaki, S., Schalch-Moser, A., Zumthor, L., Manfredi, P., Ebbensgaard, A., Schirmer, T., and
701 Jenal, U. (2014). Activation and polar sequestration of PopA, a c-di-GMP effector protein
702 involved in Caulobacter crescentus cell cycle control. Molecular microbiology *94*, 580-594.
703
704 Park, K.T., Dajkovic, A., Wissel, M., Du, S., and Lutkenhaus, J. (2018). MinC and FtsZ mutant
705 analysis provides insight into MinC/MinD-mediated Z ring disassembly. The Journal of
706 biological chemistry *293*, 5834-5846.
707
708 Perez, A.M., Mann, T.H., Lasker, K., Ahrens, D.G., Eckart, M.R., and Shapiro, L. (2017). A
709 Localized Complex of Two Protein Oligomers Controls the Orientation of Cell Polarity. mBio *8*.
710 Preibisch, S., Saalfeld, S., and Tomancak, P. (2009). Globally optimal stitching of tiled 3D
711 microscopic image acquisitions. Bioinformatics (Oxford, England) *25*, 1463-1465.
712
713 Ptacin, J.L., Gahlmann, A., Bowman, G.R., Perez, A.M., von Diezmann, A.R., Eckart, M.R.,
714 Moerner, W.E., and Shapiro, L. (2014). Bacterial scaffold directs pole-specific centromere
715 segregation. Proc Natl Acad Sci U S A *111*, E2046-2055.
716
717 Radhakrishnan, S.K., Thanbichler, M., and Viollier, P.H. (2008). The dynamic interplay between
718 a cell fate determinant and a lysozyme homolog drives the asymmetric division cycle of
719 Caulobacter crescentus. Genes & development *22*, 212-225.
720
721 Schindelin, J., Arganda-Carreras, I., Frise, E., Kaynig, V., Longair, M., Pietzsch, T., Preibisch,
722 S., Rueden, C., Saalfeld, S., Schmid, B.*, et al.* (2012). Fiji: an open-source platform for
723 biological-image analysis. Nature methods *9*, 676-682.
724
725 Schrader, J.M., Li, G.-W., Childers, W.S., Perez, A.M., Weissman, J.S., Shapiro, L., and
726 McAdams, H.H. (2016). Dynamic translation regulation in Caulobacter cell cycle control.
727 Proceedings of the National Academy of Sciences *113*, E6859-E6867.
728
729 Shapiro, L., Agabian-Keshishian, N., and Bendis, I. (1971). Bacterial differentiation. Science
730 (New York, NY) *173*, 884-892.

731 Shen, X., Collier, J., Dill, D., Shapiro, L., Horowitz, M., and McAdams, H.H. (2008).
732 Architecture and inherent robustness of a bacterial cell-cycle control system. Proc Natl Acad Sci
733 U S A *105*, 11340-11345.
734
735 Thanbichler, M., and Shapiro, L. (2006). MipZ, a spatial regulator coordinating chromosome
736 segregation with cell division in Caulobacter. Cell *126*, 147-162.
737
738 Tsokos, C.G., and Laub, M.T. (2012). Polarity and cell fate asymmetry in Caulobacter
739 crescentus. Current opinion in microbiology *15*, 744-750.
740
741 Tsokos, C.G., Perchuk, B.S., and Laub, M.T. (2011). A Dynamic Complex of Signaling Proteins
742 Uses Polar Localization to Regulate Cell-Fate Asymmetry in Caulobacter crescentus.
743 Developmental Cell *20*, 329-341.
744
745 Van der Henst, C., de Barsy, M., Zorreguieta, A., Letesson, J.J., and De Bolle, X. (2013). The
746 Brucella pathogens are polarized bacteria. Microbes and infection *15*, 998-1004.
747
748 Viollier, P.H., Sternheim, N., and Shapiro, L. (2002). Identification of a localization factor for
749 the polar positioning of bacterial structural and regulatory proteins. Proc Natl Acad Sci U S A
750 *99*, 13831-13836.
751
752 Walsh, I., Martin, A.J., Di Domenico, T., Vullo, A., Pollastri, G., and Tosatto, S.C. (2011).
753 CSpritz: accurate prediction of protein disorder segments with annotation for homology,
754 secondary structure and linear motifs. Nucleic Acids Res *39*, W190-196.
755
756 Yeh, Y.C., Comolli, L.R., Downing, K.H., Shapiro, L., and McAdams, H.H. (2010). The
757 caulobacter Tol-Pal complex is essential for outer membrane integrity and the positioning of a
758 polar localization factor. Journal of bacteriology *192*, 4847-4858.
759

760 **Acknowledgements.** We thank Jared Schrader for providing critical reviews of the manuscript.

761 We also thank Lucy Shapiro for providing critical *C. crescentus* strains that supported this study.

762 **METHODS**

763 **Phase Contrast, DIC, and Epifluorescence Microscopy**

764 Cells were imaged after being immobilized on a 1.5% agarose pad containing corresponding

765 inducers when required. Phase microscopy was performed by using a Nikon Eclipse T*i*-E

766 Inverted microscope equipped with an Andor Ixon Ultra DU897 EMCCD camera and a Nikon

767 CFI Plan-Apochromat 100X/1.45 Oil objective. DIC microscopy was performed using the same

768 microscope and camera but with a Nikon CFI Plan-Apochromat 100X/1.45 Oil DIC objective
769 with a Nikon DIC polarizer and slider in place. Excitation source was a Lumencor SpectraX light
770 engine. Chroma filter cube CFP/YFP/MCHRY MTD TI was used to image ECFP (465/25M),
771 EYFP (545/30M), and mCherry (630/60M). Chroma filter was used to image EGFP and sfGFP
772 (470/40X, 515/30M). Chromosomal DNA was visualized by using 1.5 µg/ml DAPI. DAPI was
773 imaged using 395/25X, 435/26M Chroma filter set. Images were collected and processed with
774 Nikon NIS-Elements AR software.

775 **Time-lapse Microscopy**

776 sfGFP-PodJ, mcherry-PopZ, SpmX-mcherry, or CFP-ParB was tracked using phase and
777 fluorescence microscopy. Images were collected every 1-3 min over the course of 1-2 cell
778 division (~4 h). The imaging system used was Nikon Eclipse T*i*-E microscope equipped with an
779 Andor Ixon Ultra DU897 EMCCD camera and NIS-Elements software. *C. crescentus* cells with
780 corresponding expression gene were grown to the early-log phase in M2G or PYE medium
781 (OD_{600} = 0.2), and then induced by xylose or vanillic acid for 2 hours prior to synchronization.
782 Swarmer cells were isolated from the culture by centrifugation (20 mins at 11,000 rpm, 4°C)
783 after mixture with 1 volume of Percoll (GE Healthcare). The synchronized swarmer cells were
784 pipetted onto an agarose (2%) pad containing medium with inducers, and sealed with wax.
785 During time lapse experiments, phase and fluorescence images were taken in 1 min intervals for
786 sfGFP-PodJ, mcherry-PopZ, and SpmX-mcherry. Phase and fluorescence images were taken in 3
787 min intervals for CFP-ParB.

788 **Purification of PodJ, PopZ, SpmX, and PleC Variants**

789 Protein expression of all PodJ variants followed the same protocol and is described in detail
790 below for the PodJ (1-635). To purify the cytoplasmic portion of PodJ(1-635), Rosetta (DE3)
791 containing plasmid pwz091 was grown in 6 liters LB medium (20 µg/ml chloramphenicol and
792 100 µg/ml ampicillin) at 37°C. The culture was then induced at an OD_{600} of 0.4–0.6 with 0.5
793 mM IPTG overnight at 18°C. The cells were harvested, resuspended in the lysis buffer (50 mM
794 Tris-HCl, 700 mM KCl, 20 mM Imidazole, 0.05% dextran sulfate, pH 8.0), in the presence of
795 protease inhibitor cocktail tablets without EDTA (Roche).

796 The cell suspension was lysed with three passes through an EmulsiFlex-C5 cell disruptor
797 (AVESTIN, Inc., Ottawa, Canada), and the supernatant was collected by centrifuging at 13000 *g*
798 for 30 min at 4°C. In addition, the insoluble cell debris was resuspended by the recover buffer
799 (50 mM Tris-HCl, 1000 mM KCl, 20 mM Imidazole, 0.05% dextran sulfate, pH 8.0) and its
800 supernatant was collected as well as the previous centrifugation. The combined supernatants
801 were loaded onto a 5 ml HisTrap™ HP column (GE Healthcare) and purified with the ÄKTA™
802 FPLC System. After washing with 10 volumes of wash buffer (50 mM Tris-HCl, 300 mM KCl,
803 and 25 mM imidazole, pH 8.0), protein was collected by elution from the system with elution
804 buffer (50 mM Tris-HCl, 300 mM KCl, and 500 mM imidazole, pH 8.0), and concentrated to a 3
805 ml volume using Amicon Centrifugal Filter Unites, resulting in > 95% purity. All PodJ variants
806 were dialyzed with a buffer containing 50 mM Tris-HCl (pH 8.0), 300 mM KCl, and then
807 aliquoted to small volume (100 µl) and kept frozen at -80°C till use.

808 His-SpmX (1-365) REF and His-PleC_PASCD expression and purification followed the same
809 protocol except using a different lysis buffer (50 mM Tris-HCl, 300 mM KCl, 20 mM Imidazole,
810 pH 8.0) and without recover step as in PodJ purification. His-PopZ was expressed and purified
811 the same as described (Ptacin et al., 2014).

Size Exclusion Chromatography and Native Gel Assay

A gel filtration standard (Sigma) containing thyroglobulin (bovine, 669 kDa), carbonic anhydrase (bovine, 29 kDa), blue dextran (2,000 kDa), apoferritin (horse, 443 kDa), β-Amylase (sweet potato, 200 kDa), alcohol dehydrogenase (yeast, 150 kDa), and albumin (bovine, 66 kDa) were used to generate a molecular weight standard plot using a Superdex 200 10/300 GL column (GE Healthcare). A 3.2 mg/ml sample of His-PodJ(1-635) was loaded onto the column and eluted after 7.9 ml, 12.8 ml, and 15.0 ml of buffer, corresponding to a molecular weight of 1,851 kDa, 194 kDa, and 70.7 kDa (theoretical monomer = 73.0 kDa). One representative result of triplicates was shown.

His-PodJ(1-635) was also analyzed by running a native gel. Protein was separated by gel electrophoresis (8% separate gel) at 80 V for at least 4 hours at 4^{o}C (ref), using a Native protein ladder (range from 66 to 669 kDa, Thermo Fisher).

Fluorescence Polarization Assay

To label PodJ_PSE (471-635) and PodJ_CC4-6 (250-430), we cloned a cysteine just after the 6X His tag of these two proteins at the N-terminal. PodJ_PSE (Cys) and PodJ_CC4-6 (Cys) expression and purification followed the same protocol as PodJ mentioned above. These two proteins were labeled at the cysteine using thiol-reactive BODIPY™ FL N-(2-Aminoethyl) Maleimide (Thermo Fisher). The proteins were mixed together with 10-fold excess BODIPY™ FL N-(2-Aminoethyl) Maleimide and allowed to react for 2 hours at room temperature, and the unreacted dye was quenched with mercaptoethanol (5% final concentration). The labelled proteins were purified via dialysis to remove unreacted fluorescent dye (5 times, 500 ml buffer and 30 mins each).

834 Fluorescence polarization binding assays were performed by mixing 100 nM labeled proteins
835 with 0, 0.25, 0.5, 1, 2, 4, 8, 16 μM partner protein (PopZ, SpmX, PleC, or BSA) for 45 minutes
836 to reach binding equilibrium at the room temperature. Fluorescent Proteins were excited at 470
837 nm and emission polarization was measured at 530 nm in an UV-vis Evol 600
838 spectrophotometer (Thermo). Fluorescent polarization measurements were performed in
839 triplicates, and three independent trials were averaged with error bars representing the standard
840 deviation.

841 **Western Blot**

842 Western blot analysis was used to determine if PodJ was excreted from cells upon
843 overexpression of SpmX and in Δ*popZ* strains. Cells were grown in 30 ml PYE medium to early-
844 log phase and induced by appropriate inducer for 3 hours at 30°C. Cells were harvested at
845 OD600 about 0.6 (4,000 *g*, 10 min) and resuspended using 5 ml PYE medium, and the
846 supernatants were also collected. Next, cells were removed from supernatants by filtration using
847 a 0.45 μm pore membrane (GE Healthcare). The supernatants containing excreted PodJ were
848 then condensed into 1 ml by additional centrifugation (30,000 *g*, 60 min). The presence of
849 purified PodJ foci from media supernatants were confirmed by observing PodJ foci using
850 epifluorescence microscopy.

851 Both cells and their supernatants were lysed by heating (100°C for 30 min) with protein sample
852 buffer. Approximately 5-μg protein from cell samples and the same volume samples from
853 supernatants were loaded on and separated by 12% SDS–PAGE. Proteins were transferred onto
854 PVDF membranes (GE Healthcare) and standard western blotting procedures (Li et al., 2015)
855 were followed. The anti-GFP antibody (Cell Signaling Technology) and anti-CtrA antibody (gift

from Lucy Shapiro) with 1:1000 dilution was used to determine the distribution of sfGFP-PodJ and CtrA in/out of the cell, respectively. PVDF membranes were treated with an ECL western blotting kit (ThermoFisher) and visualized using a ChemiDoc XRS+ system (Bio-Rad).

Flow Cytometry

Strains analyzed were grown overnight in PYE under antibiotic selection pressure at 28ºC. Cells were diluted to an OD_{600} of 0.1 in PYE/antibiotic and induced with 0.03% xylose for 4 hours, if applicable. Rifampicin (20 µg/mL) was then added and cells were grown for 3 more hours to allow for complete replication of DNA. Cells were then fixed in cold, 70% ethanol overnight at 4ºC for up to one week by adding 700 µL of 200 proof ethanol to 300 µL of cell culture. To stain, cells were collected by centrifugation at 6,000g for 2 minutes and resuspended in 1mL of Tris-HCl buffer (20mM Tris-HCl, pH=7.5, 150mM NaCl) containing 0.2 µg/mL RNase (RNase A, 10 mg/mL, ThermoFisher) and 1µM SYTOX Green nucleic acid stain. Cells were incubated at room temperature for 15 minutes then samples were run on a Cytoflex S (Beckman-Coulter) using 488 nm laser with a FitC filter (525 nm). Cells were selected using FSC-H and SSC-H gained to 10 and 20, respectively. Cells were thresholded in FitC-H at 1000. 10000 events were collected flowing at 10 µL per minute with an abort rate of less than 5%. Raw data was exported to Prism and histograms were generated.

QUANTIFICATION AND STATISTICAL ANALYSIS

FIJI/ImageJ ((Schindelin et al., 2012);(Preibisch et al., 2009)) and MicrobeJ (Ducret et al., 2016) were used for image analysis. Number of replicates and number of cells analyzed per replicate are specified in corresponding legends. All experiments were replicated at least 2 times, and statistical

878 comparisons were carried out using GraphPad Prism with two-tailed Student's t tests. Differences
879 were considered to be significant when *p* values were below 0.05. In all figures, measurements are
880 shown as mean ± standard deviations (s.d.).

881 **Kymograph Analyses**

882 Kymographs of fluorescence intensity were obtained by using the built-in kymograph function of
883 the Microbe-Tracker in MicrobeJ(Ducret et al., 2016). The signal of background was subtracted
884 before the kymograph analysis, and the observation of stalk at the pole of *C. crescentus* cell was
885 defined as the old pole. The predivisional cell was selected as the start point cells in Figure 1C
886 and Figure 4G. In Figure 1C, another round of kymograph analysis was performed after the first
887 cell division. The new pole **b** became to be the old pole after cell division and another two new
888 pole (**c** and **d**) were formed.

889 **Intrinsically Disordered Region Analysis**

890 The probability of intrinsic disorder region over the primary sequence of PodJ was predicted by
891 three independent programs, *i.e.*, Metadisorder MD2(Kozlowski and Bujnicki, 2012) SPOT
892 (Hanson et al., 2017), and Cspritz(Walsh et al., 2011). The average scores of these programs were
893 plotted against the PodJ sequence. We assumed the region as an intrinsic disorder with the
894 probability > 75% in this study.

895

896 **Recruitment index measurement**

897 The recruitment index in Figure 3B is calculated using the formula below similar as previous
898 described(Holmes et al., 2016).

899 $$\text{Relative recruitment index (\%)} = \frac{a - b - c}{a - c}$$

900 Here, *a* is the sum of the fluorescent signal within all the cell meshes, *b* is the sum of the
901 fluorescent signal in the middle of cells, and *c* is the background fluorescence.
902
903 **Calculation of Subcellular Co-Localization with PodJ variants**
904 To measurement of the co-localization ratio in Figure 3C, Figure 5C, Figure 6C, and Figure S3,
905 we used strict criteria to calculate how the proteins interaction with the PodJ variants, *i.e.,* (I), the
906 localization patterns of the interaction proteins are changed after co-expression. (II), the two
907 proteins are 100% co-localized at the pole (binding), or drive each other apart from the pole
908 (dispersion). Failure of either of these two criteria means the interaction of the two proteins is
909 undetermined. About 200 cells were calculated for each interaction sets.
910 **Supplementary Figure Captions**
911 **Figure S1:** (A) Time-lapse imaging of sfGFP-PodJ induced by 0.003% xylose after two rounds
912 of cell division. (B) sfGFP-PodJ accumulates at the new cell pole in stalk and predivisional cells.
913 During the swarmer to stalked cell transition sfGFP-PodJ diminishes at the old cell pole.
914
915 **Figure S2:** Analysis of PodJ domain deletion library when expressed alone heterologously in *E.*
916 *coli* or co-expressed with PopZ, SpmX or PleC fluorescent protein fusions. Solid circles indicate
917 co-localization of PodJ variants together with PopZ, SpmX or PleC. Open circles indicate PodJ
918 variants that do not co-localize with PopZ, SpmX or PleC. Question marks indicate no
919 assignment can be made based upon the co-expression assay.
920
921 **Figure S3:** (A) Analysis table of PodJ co-expression with potential client proteins in *E. coli*.
922 (B) Co-expression of YFP-PodJ together with inclusion body protein A (IbpA-mChy) indicates

that PodJ does not co-localize with inclusion bodies in *E. coli.* (C) Three potential PodJ protein-protein interaction partners (TipN, FtsZ and SpmX) promoted dispersion of YFP-PodJ when co-expressed in *E. coli.* (D) Co-expression of YFP-PodJ together with new cell pole associated proteins (PleD, DivL, DivK, CckA) indicate that these proteins do not co-localize when expressed in *E. coli.*

Figure S4: Subcellular localization pattern of *Ppopz-mCherry-popZ* in wild-type, *ΔpodJ*, and *ΔpodJ xylX::sfGFP-podJ* strains in the presence of 0.03% xylose in *C. crescentus* (A) pre-divisional cells and (B) newborn swarmer cells just after cell division. (C) Expression of mcherry-PopZ in BL21 *E. coli* indicates that PopZ accumulates randomly as a single focus at either the old or new cell poles.

Figure S5: Heterologous co-expression of PleC together with 3 new cell-pole associated scaffolds (PopZ, PodJ, and TipN). These assays indicate that PleC can be directly recruited to the cell pole by PodJ, while PleC is indirectly associated with the PopZ and TipN scaffold proteins.

Figure S6: (A) SpmX domain deletion library when expressed alone heterologously in *E. coli,* or co-expressed with PodJ fluorescent protein fusions. Dispersion of YFP-PodJ from the cell pole binding site requires the transmembrane domain of SpmX. The N-terminal fluorescent protein fusion of SpmX(1-356) disrupts its capability to accumulate as a focus suggesting that the N-terminus of SpmX may be involved in self-assembly. The SpmX-PodJ interaction requires both the lysozyme and proline-rich domains of SpmX. (B) Select PodJ domain deletion library

946 variants when expressed alone heterologously in *E. coli* or co-expressed with SpmX or
947 SpmXΔTM fluorescent protein fusions. These results suggest that PodJ's PSE and CC4-6
948 domains are sites of interaction with SpmX.
949
950 **Figure S7.** The PopZ-PodJ interaction anchors PodJ in the cytoplasm and prevents PodJ cellular
951 secretion. (A) PodJ is specifically secreted from *C. crescentus* strains that disrupt the PodJ-PopZ
952 interaction (PodJ ΔCC4-6), and (B) the PodJ secretion of C. crescentus requires the SpmX
953 scaffolding protein. (C and D) Full-length sfGFP-PodJ is not secreted from wild-type cells, but
954 is secreted from cells in the PopZ deletion strain (ΔPopZ). (E) Fractionated media indicates the
955 presence of sfGFP-PodJ foci in growth media strains that trigger PodJ cellular secretion. (F)
956 Western blot of analysis of sfGFP-PodJ and CtrA inside (I) and outside (O) of the cell. The
957 ΔPopZ strain exhibits the largest amount of extracellular sfGFP-PodJ, while western blot
958 controls of CtrA indicates that global cell lysis is likely not contributing to the observed PodJ
959 secreted foci.
960 Movie S1: Time-lapse imaging of sfGFP-PodJ in *C. crescentus NA1000.*
961 Movie S2. Time-lapse imaging of mcherry-PopZ in *C. crescentus NA1000.*
962 Movie S3: Time-lapse imaging of mcherry-PopZ in the *C. crescentus ΔpodJ strain.*
963 Movie S4: Time-lapse imaging of sfGFP-PodJ cellular secretion upon SpmX overexpression.

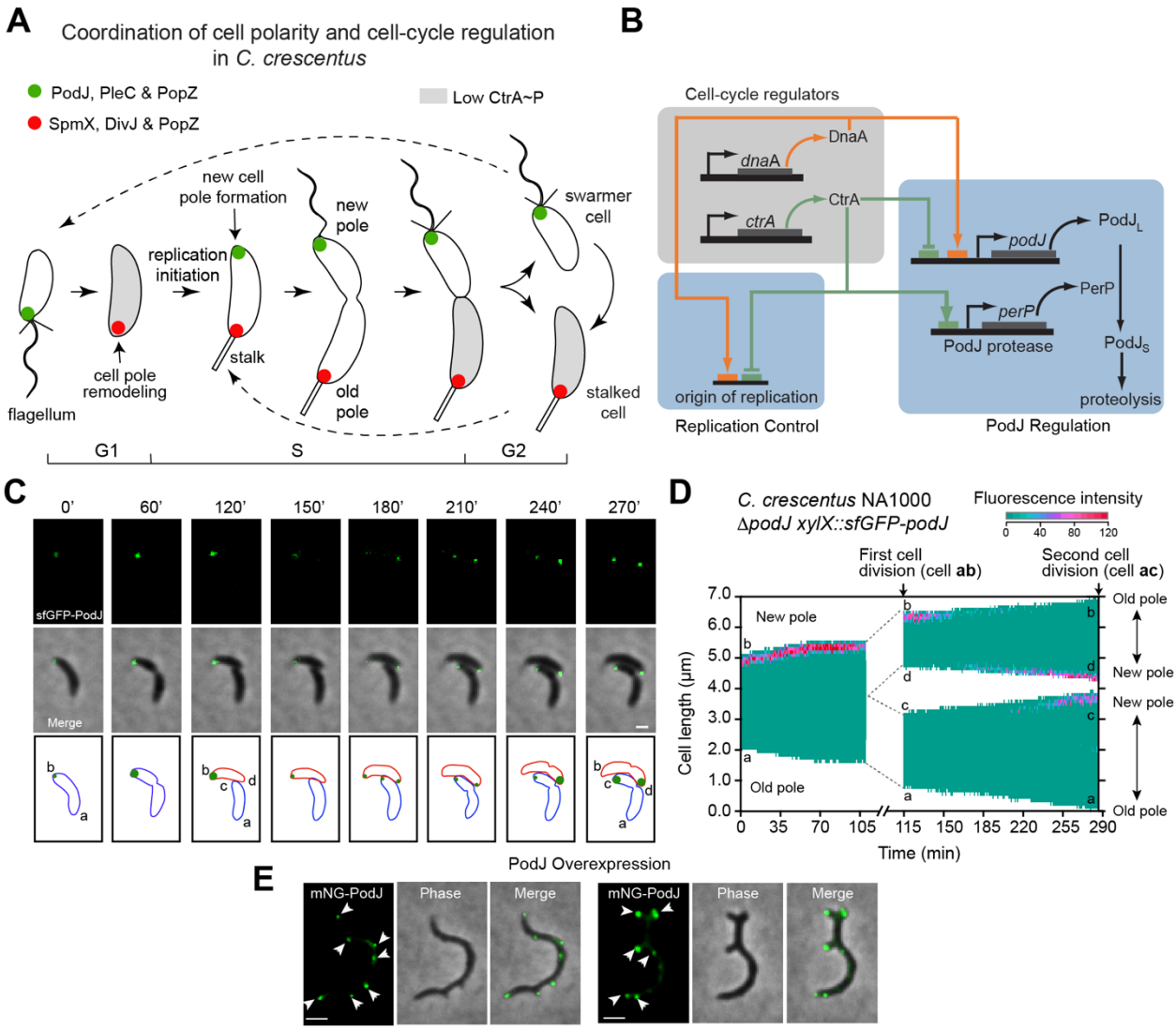

Figure 1: The scaffolding protein PodJ recognizes the new pole and is involved in cell polarity establishment. (A) Schematic of cell polarity establishment and cell cycle regulation in *Caulobacter crescentus*. Swarmer cells differentiate into stalked cells, which is correlated with cell pole remodeling of a PodJ-rich signaling hub (green) into a SpmX-rich signaling hub (red). In stalked cells, after initiation of replication a PodJ-rich signaling hub accumulates at the new cell pole. Cell division results in a swarmer cell that involved unequal inheritance of a PodJ-rich signaling hub in swarmer cells and a SpmX-rich signaling hub in stalked cells. (B) Two key cell-cycle regulators, CtrA and DnaA, co-regulate the initiation of replication and the transcription of PodJ and a PodJ specific protease PerP (C and D) Time-lapse microscopy analyses show PodJ accumulates at the new cell pole during the cell cycle. Kymographs of sfGFP-PodJ signal along the cell length over time after the synchronization of WSC1201 swarmer cells, images were acquired every 2 min. (E) Constitutive overnight PodJ overexpression (0.3% xylose) causes formation of ectopic cell poles that are co-localized with PodJ foci. Two representative cells are shown. All bars, 2 μm.

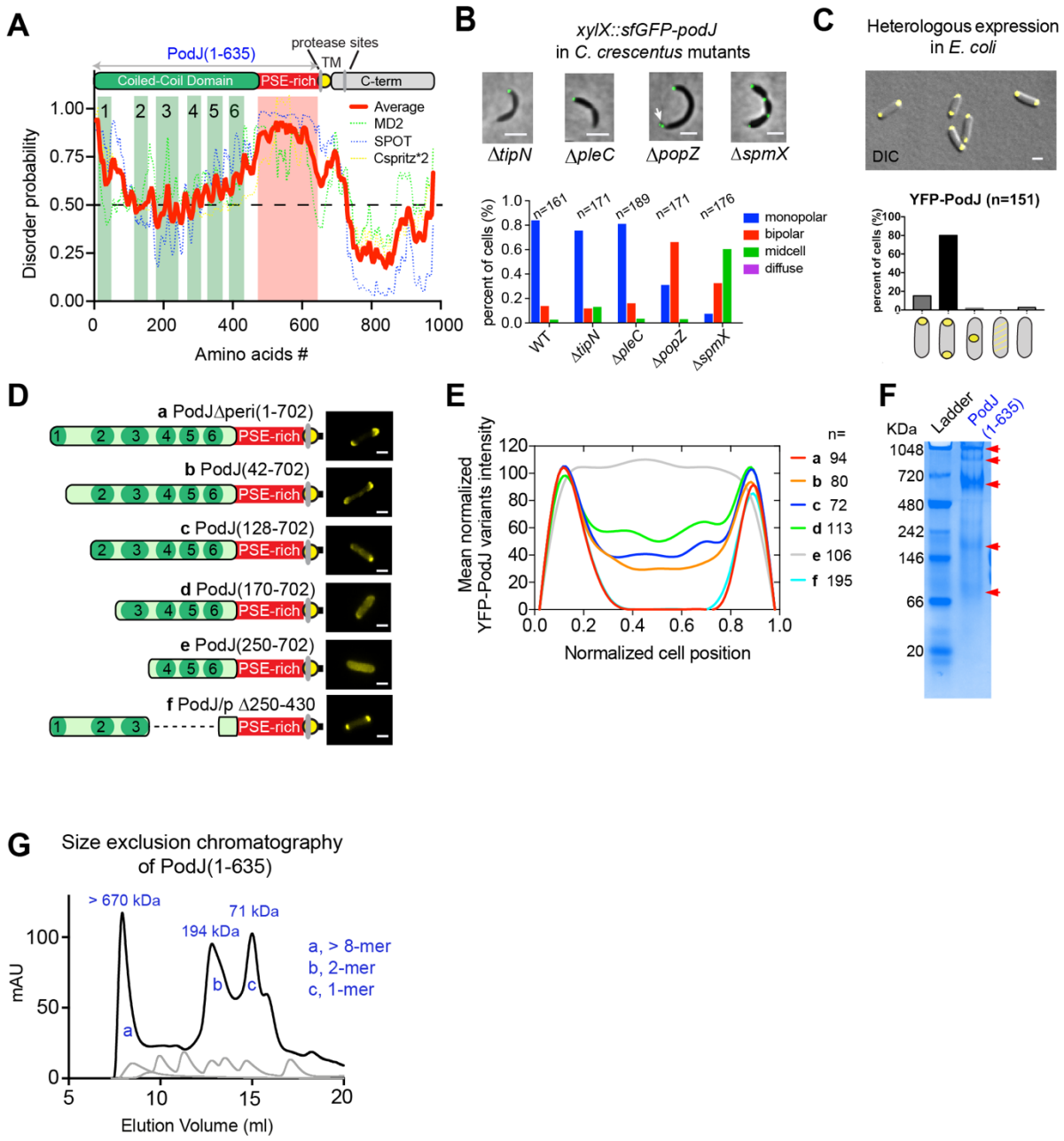

Figure 2: PodJ is a self-assembled protein, whose monopolar accumulation is dependent upon PodJ and SpmX. (A) PodJ domain organization predicted by HHpred and adapted from previous studies(Curtis et al., 2012; Lawler et al., 2006) The coiled-coil rich region was analyzed by PCOILS and modeled with MODELLER. The probability of intrinsic disorder over the primary sequence of PodJ (red line), represented as the average scores from four disorder prediction algorithms: Meta disorder MD2, SPOT, Cspritz*2, and MFDp2. (B) PodJ accumulation as a concentrated focus in *C. crescentus* cells is independent of TipN, PleC, PopZ and SpmX. However, PodJ monopolar subcellular accumulation is dependent upon the PopZ and SpmX scaffolds. (C) Subcellular localization of PodJ when heterologously expressed YFP-PodJ in *E. coli*.

(D) Heterologous expression of YFP-PodJ variants in *E. coli* reveals that the N-terminal coiled-coil region 1-3 is critical for accumulation of PodJ at the cell poles. (E) The signal of YFP-PodJ along the cell length was plotted for the cells shown in Figure 2D. All of the data was normalized with the highest intensity in each strain setting as 100%. (F) Purified PodJ(1-635) was analyzed *in vitro* via native gel analysis. The protein is subjected to nondenaturing gel electrophoresis at 4°C and subsequently stained with Coomassie blue stain. Four distinct bands indicate PodJ oligomers larger 480 kDa. (G) Analytical size exclusion chromatography was used to measure the apparent molecular mass of purified PodJ(1-635) (black line), by plotting absorbance at 215 nm versus elution volume. The indicated molecular masses of each peak were determined by comparison to the elution volume of protein standards (grey lines). A representative trace is shown from three independent replicates.

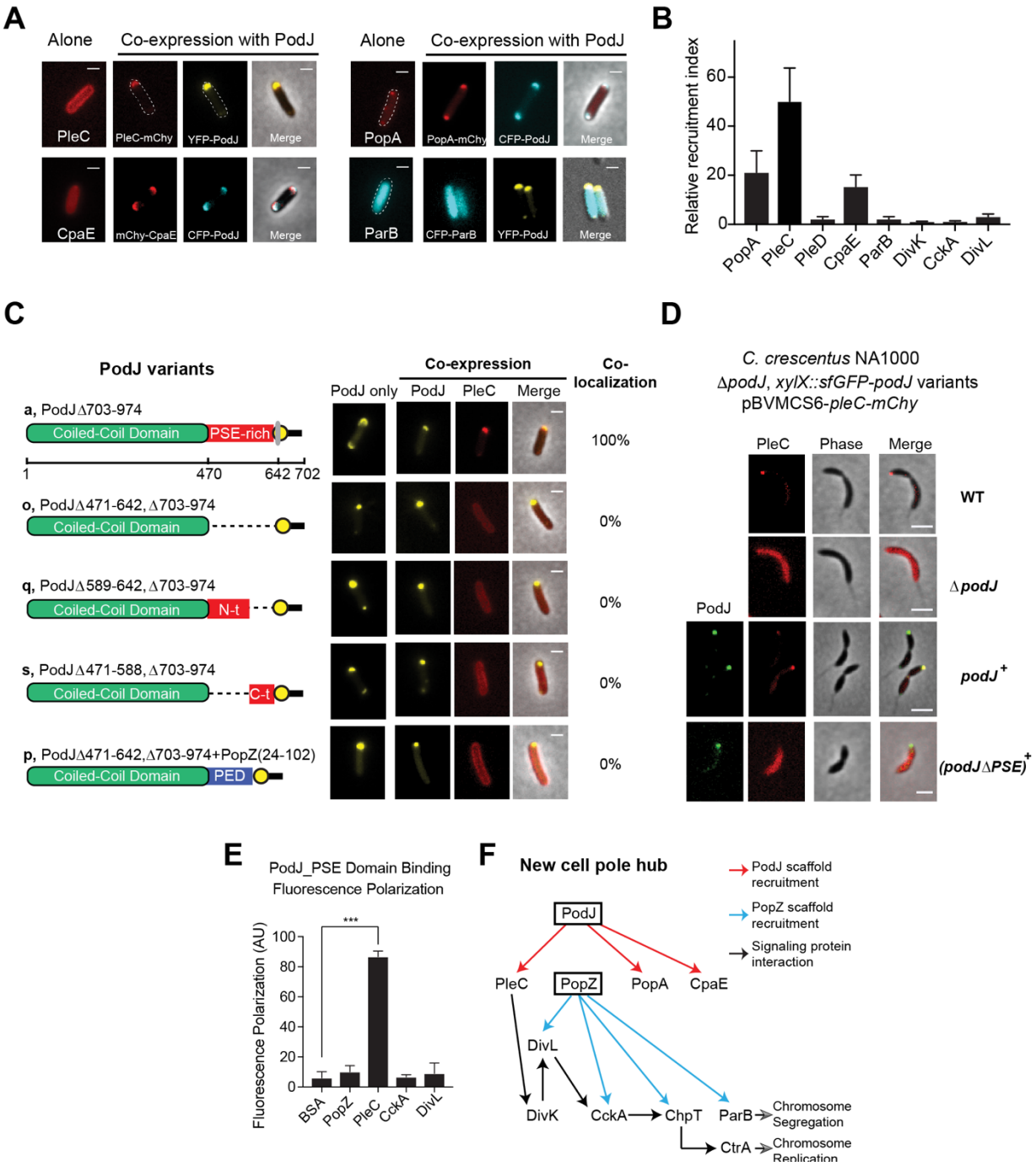

Figure 3: PodJ is a central organizer of the new cell pole signaling hub. The interactions between PodJ and binding partners were evaluated through heterologous co-expression in *E. coli*. (A) YFP-PodJ exhibits selective recruitment roles for the *C. crescentus* new cell pole proteins that include PleC, PopA and CpaE. (B) The polar recruitment ability by PodJ was calculated and normalized as a relative localization index. (C) Co-expression of PodJ variants together with PleC reveals that the intrinsically disordered PSE-rich domain is necessary for PleC recruitment to the cell pole in *E. coli*. (D) Expression of PodJ variants as a sole-copy in *C.*

crescentus revealed that the PSE-rich domain is required for PleC accumulation at the new cell poles. (E) Fluorescence polarization binding assay confirms PodJ directly interaction with PleC. 100 nM BODIPY dye labeled PodJ_PSE mixed with the following new cell pole proteins at 10 μM PopZ, PleC, CckA and DivL. PodJ_PSE specifically binds to PleC. (G) New cell pole localization hierarchy based upon these studies indicate that PodJ is a central organizer in addition to PopZ(Holmes et al., 2016) for the new cell pole signaling hub. Interactions identified in this study (red), and those discovered previously by Holmes et al. (blue)(Holmes et al., 2016).

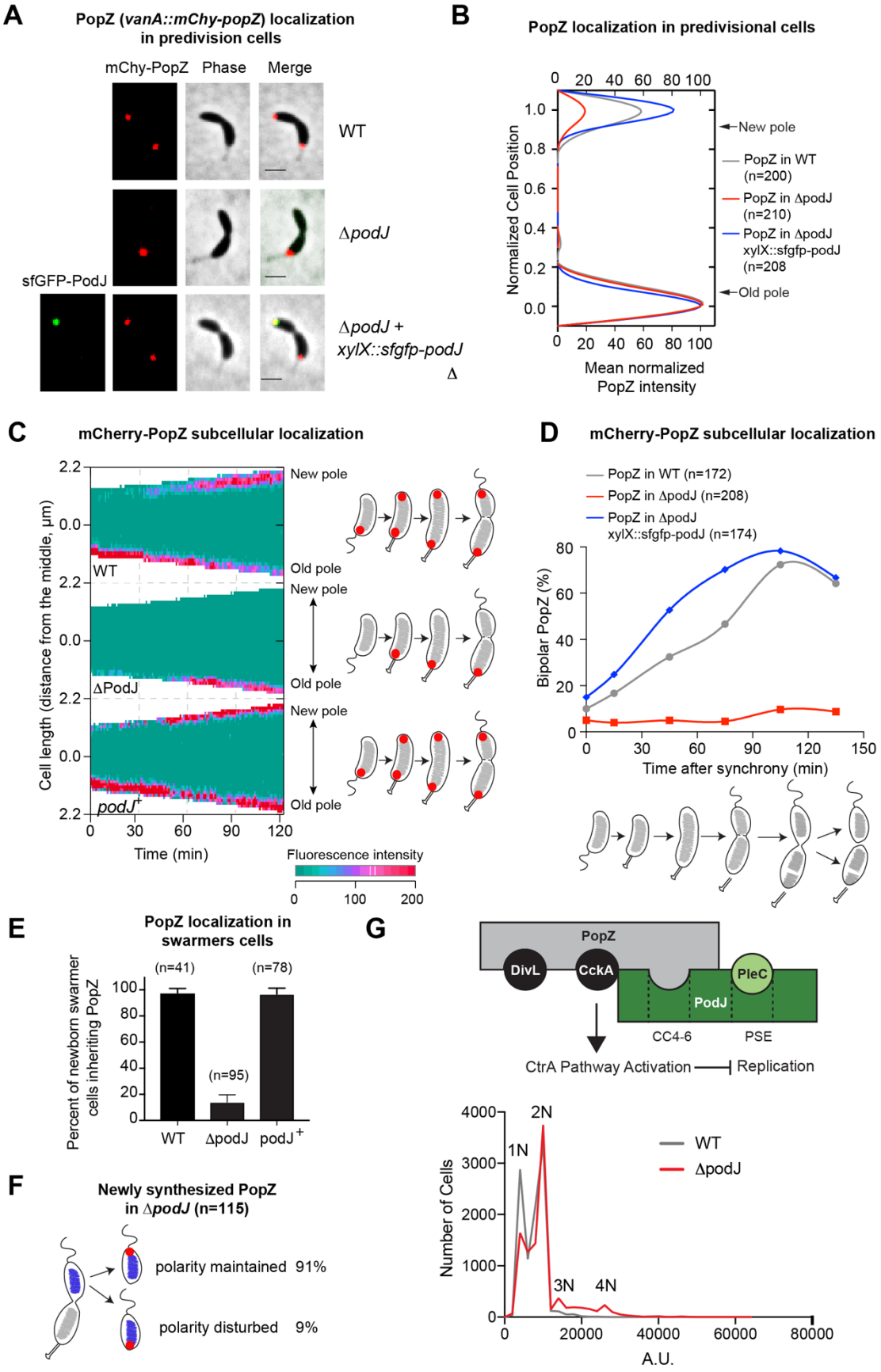

Figure 4: **PodJ nucleates PopZ assembly at the new cell pole and promotes robust inheritance of PopZ in daughter swarmer cells.** (A) mCherry-PopZ localization in predivisional cells in the wild-type (bipolar) versus the *podJ* deletion *C. crescentus* (monopolar). Bars, 2 µm. (B) Population analysis reveals a substantial reduction of PopZ abundance at the new cell pole of Δ*podJ* predivisional cells. Cell poles (new or old) were distinguished and orientated manually by observation of a stalk. The signal intensity was normalized with the highest value as 100% in each strain. (C) Kymograph analyses of mCherry-PopZ signal over the time after the synchronization of WT, Δ*podJ* and *podJ* complementary cells. Vanillate (50 mM) for mChy-PopZ induction and xylose (0.03%) for sfGFP-PodJ induction were added at 1 hr prior to synchronization of the cell culture. Images were acquired every 1 min. One of three representative cells were shown for each strain. The results indicate that PopZ fails to robustly accumulate at the new cell poles prior to cell division in Δ*podJ* strain. (D) Quantification of the percentage of cells that display detectable bipolar PopZ after cell synchronization. Time course analyses were performed within 135 mins in PYE medium for WT, *podJ* and *podJ* complementary cells (more than 130 cells were calculated for each point). Robust PopZ assembly at the new cell pole is dependent upon PodJ. (E and F) Failure to localize mcherry-PopZ to the new cell pole in Δ*podJ* results in ~80% population of swarmer cells that fail to inherit PopZ. Within a subpopulation of swarmer cells (9% of cells), nascent PopZ accumulates at the incorrect cell pole switching the inherited polarity axis. A total of 40 cells were tracked by time-lapse analyses. (G) Flow cytometry analysis of wild-type versus Δ*podJ* strains. When podJ is deleted from cells (red line), cells display a decrease in 1N and 2N cells that is accompanied with an increase in 3N and 4N cells.

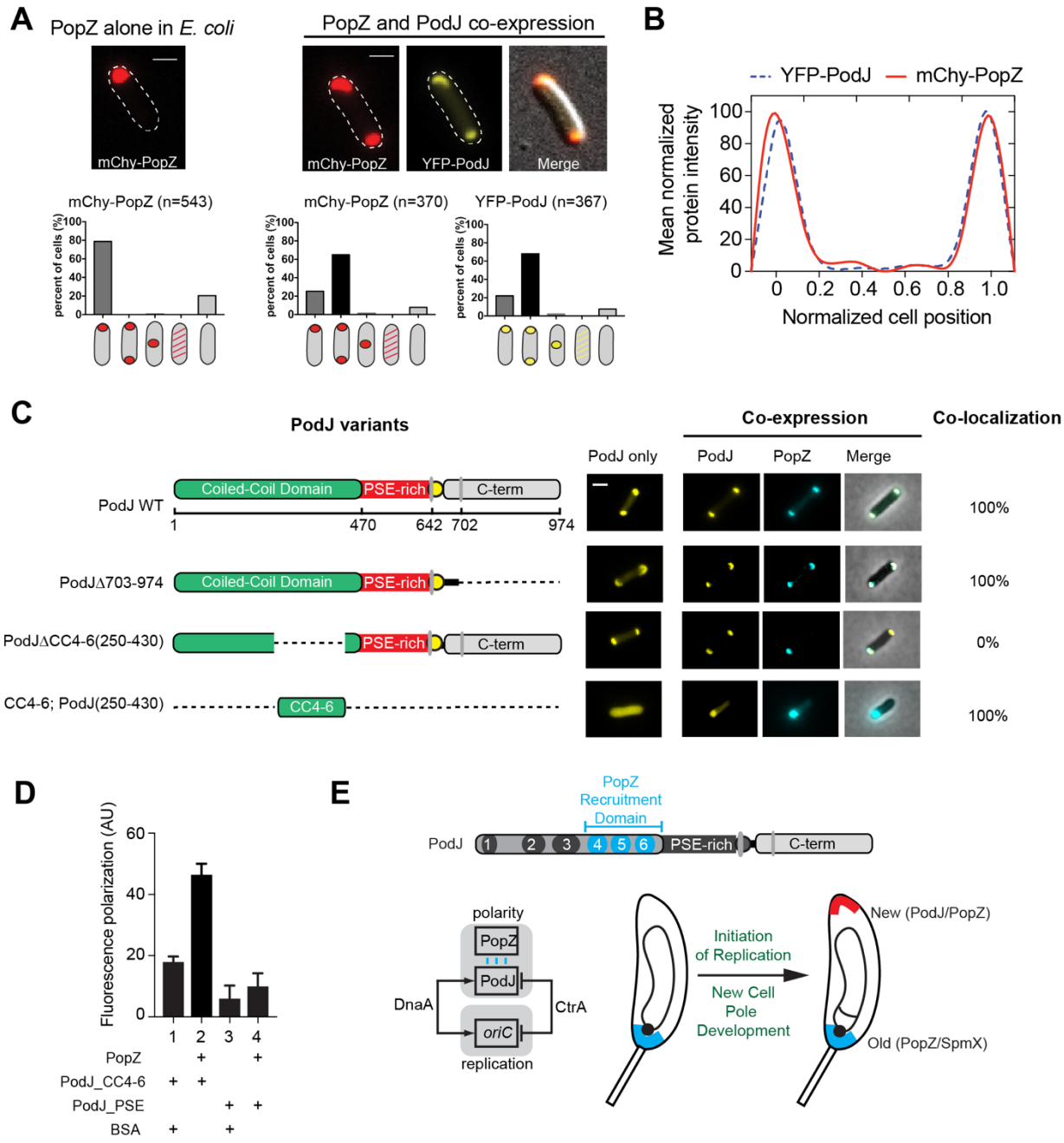

Figure 5: **PopZ binds directly to the coiled-coil 4-6 region of PodJ. (A)** Heterologous expression of YFP-PodJ and mcherry-PopZ in *E. coli*. Co-expression with PodJ causes bipolar PopZ accumulation in *E. coli*. (B) Mean protein intensity of YFP-PodJ and mcherry-PopZ versus cell length (n=370). The signal intensity was normalized with the highest value as 100% in each strain. (C) Co-expression of PodJ variants together with PopZ in *E. coli* reveals that the coiled-coil 4-6 region in PodJ is necessary for the interaction with PopZ. (D) Fluorescence polarization binding assay of the BODIPY dye labeled PodJ_PSE or PodJ_CC4-6 mixed with 10 µM PopZ, using BSA as a negative control. PopZ binds specifically to the CC4-6 domain of PodJ, however does not bind to its PSE-rich domain (E) Model for PodJ serving as a new cell pole development signal

that triggers polarity establishment upon the initiation of replication, through its cell-cycle coordinated expression and specific interaction with the PopZ scaffold. All bars, 2 µm.

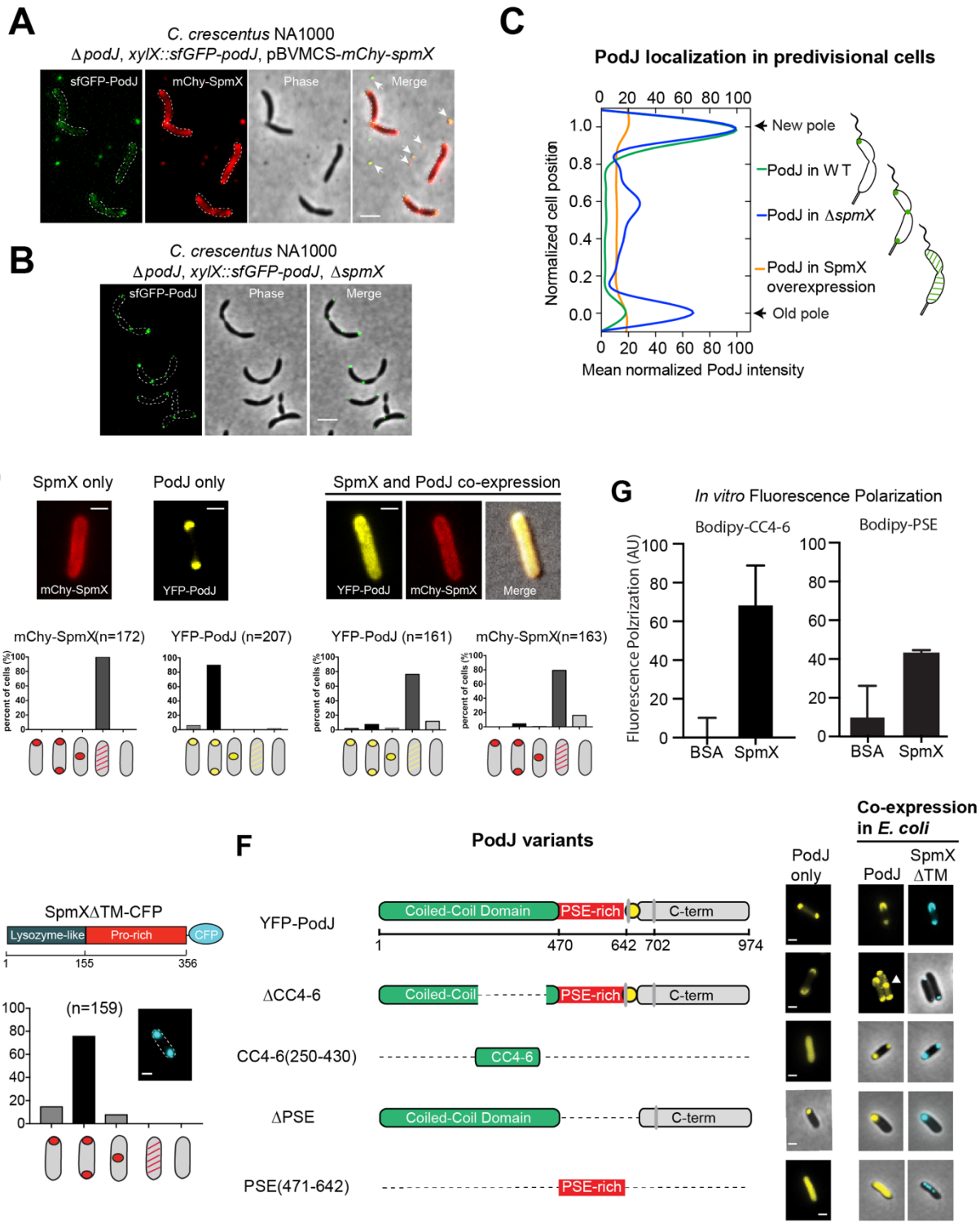

Figure 6: **SpmX is a negative regulator for cell pole accumulation of PodJ.** (A) SpmX directly or indirectly regulates PodJ subcellular localization in *C. crescentus*. Overexpression of SpmX results in a reduction of cell pole localized PodJ and secretion of PodJ from cells. (B) In the absence of SpmX, PodJ accumulates at all poles in *C. crescentus*. (C) Quantitative analysis of PodJ localization in *C. crescentus* predivisional cells in wild-type, Δ*spmX* and SpmX overexpression strains. (D) Heterologous expression of YFP-PodJ alone results in bipolar PodJ accumulation, while expression of SpmX-mcherry alone is disperse in *E. coli*. (E) Co-expression of PodJ together with SpmX causes PodJ to disperse from the cell poles in *E. coli*. All bars, 2 µm. (F) Co-expression of PodJ variants together with a SpmX variant lacking the transmembrane domain (SpmX'). These analyses indicate that SpmX's dispersal of PodJ requires the PSE and CC4-6 domains of PodJ. (G) I*n vitro* fluorescence polarization assays screening the binding interactions between SpmX and Bodipy labeled PodJ-PSE domain and PodJ-CC4-6 domains.

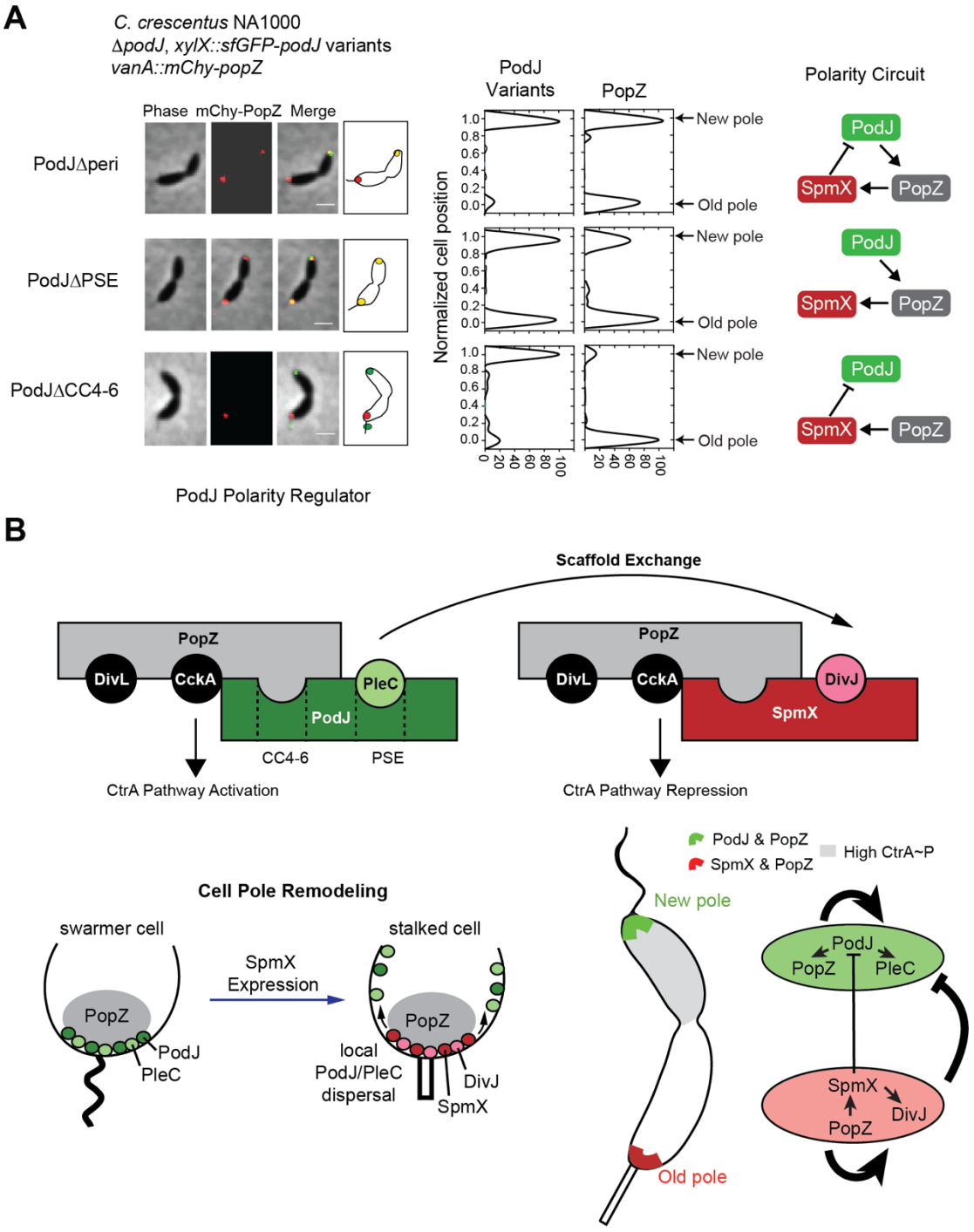

Figure 7: **A network of protein-protein regulatory interactions enable polarity establishment in *C. crescentus*** (A) A polarity circuit in which PodJ promotes PopZ new cell pole localization, PopZ promotes SpmX accumulation at the cell poles, and SpmX negatively regulates PodJ subcellular localization at the cell poles Expression of PodJ variants and PopZ as the sole copy in *C. crescentus*. The cytoplasmic domain of PodJ, containing both CC4-6 and the PSE-rich domain, supports bipolar localization of PopZ and new cell pole localization of PopZ. In contrast,

expression of PodJ∆CC4-6 results in predivisional cells that fails to accumulate PopZ at the new cell pole. Removal of the domain that is required for SpmX to disperse PodJ from the cell poles, PodJ∆PSE, results in PodJ accumulation at both cell poles in *C. crescentus*. These results indicate that the regulatory protein-protein interaction between PodJ, PopZ and SpmX are required for robust cell polarity of *C. crescentus* predivisional cells. **(B)** SpmX functions as a local negative regulator of PodJ accumulation at the old cell pole. **(C)** The establishment of the compositionally distinct new and old cell poles is driven by a network of scaffolding proteins that combines positive feedback together with inhibition.